BOREAS An international journal of Quaternary research

Detailing the impact of the Storegga Tsunami at Montrose, Scotland

MARK D. BATEMAN, TIM C. KINNAIRD, JON HILL, ROBERT A. ASHURST, JENNA MOHAN, REBECCA B. I. BATEMAN AND RUTH ROBINSON

BOREAS

Bateman, M. D., Kinnaird, T. C., Hill, J., Ashurst, R. A., Mohan, J., Bateman, R. B. I. & Robinson, R.: Detailing the impact of the Storegga Tsunami at Montrose, Scotland. *Boreas*, https://doi.org/10.1111/bor.12532. ISSN 0300-9483.

The Storegga tsunami, dated in Norway to 8150±30 cal. years BP, hit many countries bordering the North Sea. Run-ups of >30 m occurred and 1000s of kilometres of coast were impacted. Whilst recent modelling successfully generated a tsunami wave train, the wave heights and velocities, it under-estimated wave run-ups. Work presented here used luminescence to directly date the Storegga tsunami deposits at the type site of Maryton, Aberdeenshire in Scotland. It also undertook sedimentological characterization to establish provenance, and number and relative power of the tsunami waves. Tsunami model refinement used this to better understand coastal inundation. Luminescence ages successfully date Scottish Storegga tsunami deposits to 8100±250 years. Sedimentology showed that at Montrose, three tsunami waves came from the northeast or east, over-ran pre-existing marine sands and weathered igneous bedrock on the coastal plain. Incorporation of an inundation model predicts well a tsunami impacting on the Montrose Basin in terms of replicate direction and sediment size. However, under-estimation of run-up persisted requiring further consideration of palaeotopography and palaeo-near-shore bathymetry for it to agree with sedimentary evidence. Future model evolution incorporating this will be better able to inform on the hazard risk and potential impacts for future high-magnitude submarine generated tsunami events.

Mark D. Bateman (m.d.bateman@sheffield.ac.uk) and Robert A. Ashurst, Department of Geography, University of Sheffield, Winter St., Sheffield S10 2TN, UK; Tim Kinnaird, Rebecca B. I. Bateman and Ruth Robinson, School of Earth and Environmental Science, St Andrews University, St Andrews KY16 9AL, UK; Jon Hill and Jenna Mohan, Department of Environment and Geography, University of York, Heslington, York YO10 5NG, UK; *received 8th December 2020, accepted 7th April 2021.*

The Storegga tsunami event might be considered the largest natural disaster to hit countries around the North Sea during the last 10 000 years. It was caused by a submarine slide off of the continental slope of south-western Norway (Fig. 1; Haflidason *et al*. 2005) which displaced water generating a tsunami event (Harbitz *et al*. 2006). Deposits associated with the Storegga tsunami have been reported from sites as far apart as Norway, Scotland, and eastern Greenland (Fig. 1A; e.g. Dawson *et al*. 1988, 2020; Svendsen & Mangerud 1990; Bondevik *et al*. 1997, 2005a; Smith *et al*. 2004, 2007; Wagner *et al*. 2010; Fruergaard *et al*. 2015; Long *et al*. 2016). The Storegga tsunami has even been connected with the final demise of Mesolithic occupation of Doggerland in the North Sea (e.g. Weninger *et al*. 2008). Proximal sites experienced tsunami wave run-up of up to 13 m and distal sites 3–5 m (Fig. 1A; Smith *et al*. 2004; Bondevik *et al*. 2005a; Fruergaard *et al*. 2015; Rasmussen *et al*. 2018). Where localized coastal configuration caused diffraction, refraction, reflection and interference, e.g. in island archipelagos like the Shetland Islands, minimum run-ups of >30 m have been reported (Dawson *et al*. 2020). Reconstructions have calculated that some 13 600 km^2 of coastal plain in the southern North Sea, from Denmark round to Scotland (but excluding Norway), would have been vulnerable to flooding from the Storegga tsunami (Weninger *et al*. 2008). In Scotland alone, at least 600 km of coastline was thought to have been impacted with inundation extending several kilometres inland in places (Smith *et al*. 2004).

The best age estimate for the Storegga tsunami event is based on AMS radiocarbon dating of mosses ripped up by the tsunami, which directly dated the tsunami deposits to 8150±30 cal. a BP (Bondevik *et al*. 2012). As reviewed by Weninger *et al*. (2008) and Dawson *et al*. (2011), many other radiocarbon ages bracketing Storegga deposits potentially suffer from erosion of the underlying strata and redeposition of organic material within the tsunami deposit or following the event. This combined with most radiocarbon ages being measured from bulk samples and the potential for young root penetration led Dawson *et al*. (2011) to suggest they should be disregarded. As reviewed by Ishizawa *et al*. (2020), optically stimulated luminescence (OSL) dating offers an alternative approach to radiocarbon and has the potential to directly date sediment moved in the tsunami event providing that during the event the sediment eroded and deposited is exposed to sunlight (referred to as bleaching). Brill *et al*. (2012) showed for a recent (2004) tsunami deposit in Thailand unbleached residuals were low (~40 years), but this may be specific to the event and sediments involved. Whilst Gaffney *et al*. (2020) successfully directly OSL dated Storegga deposits from Dogger Bank to 8140 ±290 years, Shtienberg *et al*. (2020) applied OSL to poorly sorted palaeo-tsunami deposits, which resulted in age reversals. Careful sediment characterization and provenance of easily accessible Storegga sediments would allow a better evaluation of whether appropriate bleaching of the luminescence signal happened. If this is the case, whilst not able to achieve the age precision

DOI 10.1111/bor.12532

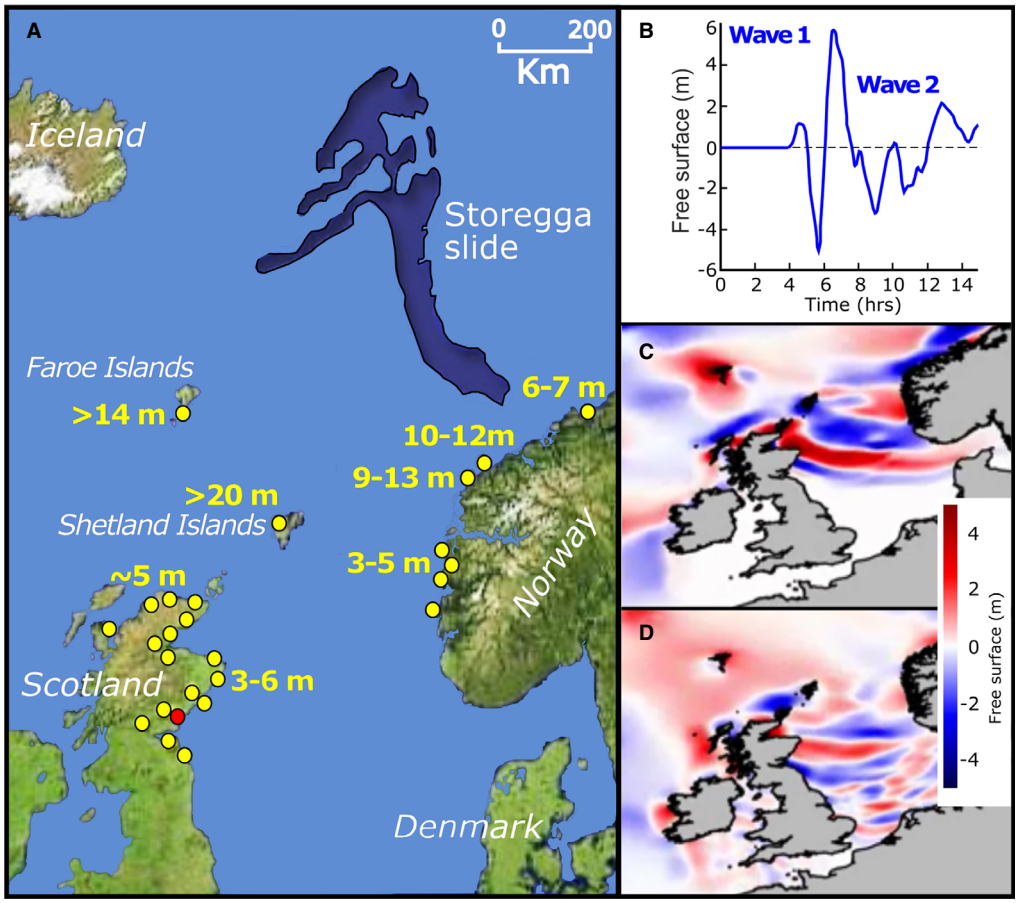

Fig. 1. The Storegga tsunami. A. Location of slide causing tsunami (based on Haflidason *et al.* 2005), location of coastal sites where tsunami deposits reported and estimated wave heights (based on Bondevik *et al.* 2005a,b; Long *et al.* 2016; Dawson *et al.* 2020). Montrose Basin in eastern Scotland shown as red circle. B. Modelled tsunami wave gauge using modern bathymetry for eastern Scotland (Hill *et al.* 2014). C and D. Modelled tsunami wave map showing distribution of first and second major waves to hit Scotland (Hill *et al.* 2014).

obtained in Norway using the AMS on moss (Bondevik *et al.* 2012), OSL would allow dating of tsunami sediments where no organic material has been preserved. OSL dating could also help to distinguish Storegga tsunami sediments from other less well-documented tsunami (e.g. Bondevik *et al.* 2005b).

Hill *et al.* (2014) presented a multiscale 3D finite element, non-hydrostatic numerical model of the tsunami generated by the Storegga slide. This assumed a simplified block sliding to trigger the event and used palaeo-bathymetry based on that of the present day adjusted for isostatic rebound using data from Bradley *et al.* (2011). Palaeo-coastlines were derived from the 0-m contour. Results were able to successfully generate a tsunami wave train (Fig. 1B), wave heights and velocities as well as plot wave movement for the equivalent of 15 h (Fig. 1C, D). At least two major waves were modelled to have impacted on Scotland (Fig. 1B, D) and a wave with an estimated 5 m run-up predicted to have over-washed most of Doggerland. Whilst very powerful, one of the acknowledged limitations of the Hill *et al.* (2014) model was it only modelled the wave up to the coastline and not any coastal inundation. Coasts were treated in the model as vertical cliffs. Thus, when model outputs of run-up were compared to run-up heights from reported inland deposits, the model tended to under-estimate. The other significant finding was that numerical resolution of near-shore bathymetry and coastline is important to minimize the difference between the modelled and geological record of run-up. Higher resolutions were not undertaken for such a large spatial area as they were computationally prohibitive.

The Storegga tsunami event is perhaps the best examined and mapped out palaeo-tsunami. As such, it holds the potential to inform present-day coastal managers to help them assess the hazard risk and potential impact for future high-magnitude submarine generated tsunami events (e.g. Jaffe *et al.* 2012; Sugawara *et al.* 2014). Future slides from the Storegga region could happen but more likely is a similar event happening from Greenland or from volcano flank collapse e.g. in the Canaries (Harbitz *et al.* 2014). The aims of this paper are to (i) establish the provenance of the tsunami sediment deposited at the type site of Maryton and in doing so

evaluate the likelihood of the OSL signal being bleached, as well as the distance sediment was moved and number of tsunami waves; (ii) directly date the deposits at Maryton using OSL to evaluate the accuracy and precision of this technique when applied to the Storegga tsunami event and improve on the existing but contested radiocarbon ages; and (iii) evolve the model of Hill *et al.* (2014) with the addition of a local inundation model and fine-tune it with the new sedimentary evidence to better estimate wave numbers, heights and velocity.

Background

Smith *et al.* (2004) comprehensively reviewed the evidence for Storegga in Scotland. The sand-layer deposited during the event was found to be comprised of coarse material at the base, overlain by fine or fine-medium sand (mean ~250 μm) ideal for OSL dating in terms of mineralogy and grain size. It is up to 1 m thick but mostly ~35 cm. Within the unit, Smith *et al.* (2004) showed that landward sites were generally finer grained reflecting dissipation of wave energy as it moved inland. They also showed fining-up successions within the deposit attributed to formation by more than one wave (Smith *et al.* 2004, 2007). The sediment laid down during the tsunami was thought to be largely from local sediment sources (Firth *et al.* 1996; Smith *et al.* 2004). Maximum water run-up was estimated at 11.1 m (Smith *et al.* 2007). Such short transport pathways in deep turbid water could provide poor opportunities for OSL bleaching.

Arguably the best evidence for the Storegga tsunami in Scotland comes from around the Montrose Basin, approximately 45 km northeast of Dundee. At present, this is a semi-enclosed inter-tidal basin formed by a barrier almost blocking the South Esk River from the North Sea (Fig. 2). The barrier is comprised of Holocene marine silts as well as dunes (Fig. 2). It is here where the first Scottish tsunami deposits were identified (Dawson *et al.* 1988) and were formally described by Gordon (1993). A total of six sites around the basin have since been reported (Smith *et al.* 2004); three to the southwest of the basin at Old Montrose, Maryton and Fullerton (Fig. 2) and three in the low lying area to the northeast of the basin at Dryleas, Dubcon and Puggieston. All but Maryton were found through coring of gullies along the maximal limits of the estuarine deposits referred to locally as carselands. The Maryton site is formed within a cliff exposure cut into the carseland (estuarine) sediments by the present tidal basin. Whilst a protected site (Site of Special Scientific Interest) it provides Scotland's only readily available place to view the Storegga tsunami deposits.

Particle size analysis of the tsunami deposits from the Montrose Basin by Smith *et al.* (2004) found at Old

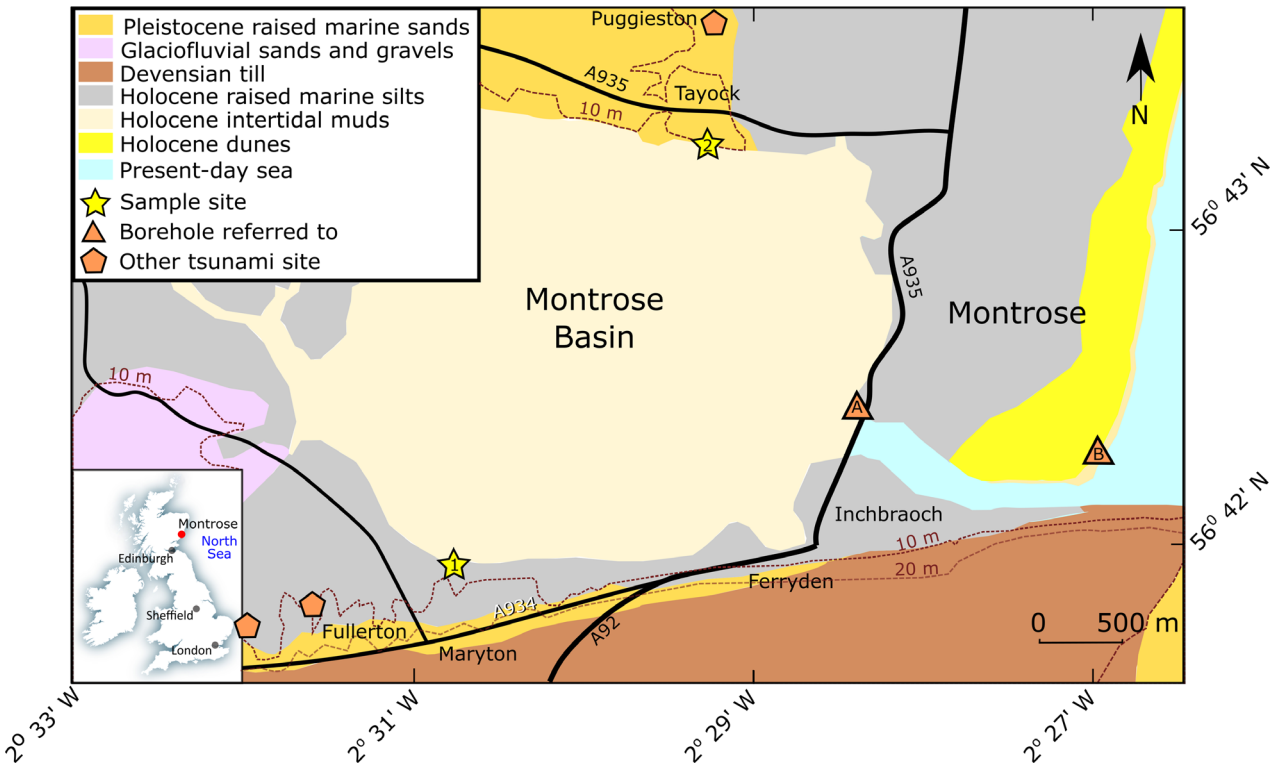

Fig. 2. The underlying superficial geology of the Montrose Basin in eastern Scotland as mapped by the British Geological Survey (Geological Map Data BGS © UKRI 2020) with study sites and previously reported other sites with Storegga tsunami deposits (from Smith *et al.* 2004). Note the Dryleas and Dubton sites are not shown but are approximately 50 and 200 m northwest of the Puggieston site.

Montrose ($n = 9$) one fining-up succession, at Maryton ($n = 11$) and Puggieston ($n = 9$) two, whilst at Fullerton ($n = 7$–18) two seaward fining-up and one landward fining-up successions were found. This suggests at least two waves entered the Montrose Basin from the sea although backwash cannot be excluded (Smith *et al.* 2004). As Table 1 shows, Maryton shows no run-up as it would have been inter-tidal at the time of the Storegga event. Run-up from the other sites indicate that the tsunami wave swept up between 1.18 and 3.93 m above the mean high water spring tide level (Table 1).

Radiocarbon dating has been carried out within the Montrose Basin on overlying and underlying peats to determine the age of the tsunami deposits here (Table 1). When recalibrated using Intcal13 (OxCal v4.3; Bronk Ramsey 2009) this dates the tsunami deposits at Puggieston between 7705±135 and 7955±195 cal. a BP (SRR2119 & 2120; Smith & Cullingford 1985). At Fullerton they date between 7760±190 and 7945±245 cal. a BP (BIRM867, 823; Smith *et al.* 1980) and at Maryton between 8120±210 and 7920±250 cal. a BP (Beta 92235, 92236; Smith *et al.* 2004). These were measured on bulk samples and appear to underestimate the Storegga event age compared to the AMS ages from Norway (Bondevik *et al.* 2012) bearing out the misgivings of Dawson *et al.* (2011).

Material and methods

Sampling

An exposure of the Storegga tsunami sediments exists in the basin edge bluff at Maryton on the southern side of the Montrose Basin (Fig. 2). In this is revealed a basal laminated pink silty clay unit grading up into a grey undifferentiated silty clay with occasional thin peat which that is believed to be the stratigraphical equivalent of the peat unit reported by Gordon (1993; Fig. 3). Above this is a sharp erosional boundary and the ~15–20 cm of the grey, micaceous, silty fine sand with iron mottling comprising the Storegga tsunami unit. Above this is a sharp erosional boundary and a grey silty clay (carse) unit attributed to be of estuarine origin (Gordon 1993). Peat between the tsunami sand and overlying estuarine silt as reported in Gordon (1993) was not observed during visits in 2007 and 2017.

Samples for luminescence dating were collected over two trips to the Maryton site. In 2007, author RR collected in opaque PVC tubes three horizontal samples from the type section: the basal unit clay unit was sampled (MARY071105-3) and, two luminescence samples (MARY071105-1 and MARY071105-2) were collected from the middle of the silty fine sand Storegga Tsunami unit (e.g. Dawson *et al.* 1988; Long *et al.* 1989). Further samples in opaque 5-cm diameter PVC tubes were collected by author MB in 2017 from the same exposure: two horizontal samples were taken from the middle of the tsunami sand unit (Fig. 3A, B; Shfd17230 and Shfd17231). A 5-cm-diameter core was also sampled vertically through the entirety of the tsunami sand unit for more detailed luminescence dating (Shfd17233–244) and sediment characterization (Fig. 3C). Further bulk samples for elemental composition and sediment characterization were collected from all the sand and estuarine silt units.

The northern edge of the Montrose Basin at Tayock is comprised of an extensive sandy bluff (Figs 2, 4A). As observed in 2019, here was up to 6 m of fine to medium moderately sorted sand. In many places, the sand showed evidence of low angle bedding some of which was rippled or in places contorted with dewatering 'involution-like' structures (Fig. 4B). British Geological Survey mapping has attributed this to be a raised terrace of Pleistocene marine sands. No evidence of estuarine silts or tsunami deposits were found at this locality. A single sample was collected for luminescence (Shfd19078) and bulk samples were collected from throughout the sand unit for elemental composition and sediment characterization. Finally, to provide end member provenance data, bulk samples were collected from the present-day beach at Montrose and from the back-beach foredunes nearby.

Sediment characterization

Provenance studies commonly use trace-element geochemistry to identify potential source sediments. Previous studies have demonstrated the effective usage of

Table 1. Storegga deposits found around Montrose Basin, their observed maximum sediment limit, adjusted height from mean high-water spring tide (MHWST) level and calculated inferred tsunami run-up (taken from Smith *et al.* 2004). Also shown are recalibrated radiocarbon ages where available.

Site	Max. observed thickness (cm)	Max observed altitude (m a.s.l.)	Adjusted (m MHWST)	Run-up (m)	Age below (cal. a BP)	Age above (cal. a BP)
Old Montrose	5	6.13	3.98	1.18	–	–
Maryton	18	4.15	2.08	0.00	7920±250	8120±210
Fullerton	44	7.87	5.98	3.93	7945±245	7760±190
Dryleas	2	6.00	3.96	1.18	–	–
Dubton	40	6.70	5.08	1.89	–	–
Puggieston	19	5.59	3.97	2.08	7955±195	7705±135

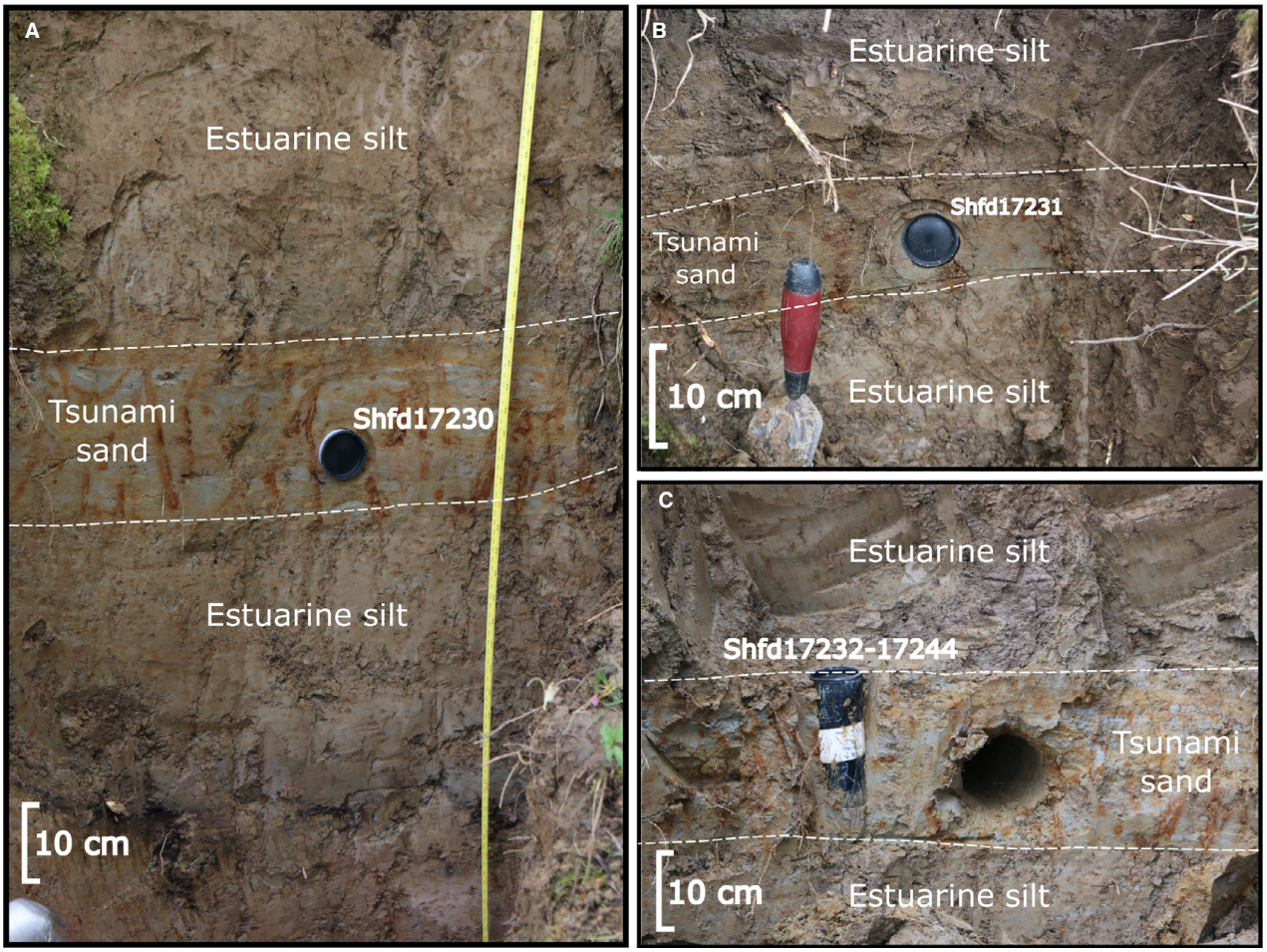

Fig. 3. Sections sampled for tsunami sediments. A. Cliff exposed at edge of Montrose Basin near Maryton sample for luminescence (MARY071105-1 to 3; Shfd17230). B. Small exposure at edge of Montrose Basin about 200 m further west also sampled for luminescence dating (Shfd17231). C. Vertical sample through tsunami sand collected from (A) for further luminescence (Shfd17232–244), particle size and ICP analysis.

relatively immobile Cr, Co, Ti, Th, Zr and Hf (latter two both from zircons) elements (e.g. Taylor & McLennan 1985; Nath *et al*. 2000; Vital & Stattegger 2000; Wolfe *et al*. 2000; Muhs & Budahn 2006; Dunajko & Bateman 2010). Provenance samples were pulverized to a fine powder using a Tema mill, then homogenized before subsampling. Samples underwent 50 element analysis by ICP-MS and ICP-OES at SGS laboratories, Canada.

Sediment particle size is also widely used to provide information on sediment transportation and deposition histories (e.g. Gale & Hoare 1991). Given that previous work, based on relative few samples, had indicated presence of potentially more than one fining-up succession, a high-resolution approach with 75 samples (60 from through the tsunami deposit) was adopted for this study. All samples from the 2017 exposure, therefore, underwent particle size analysis using a Horiba LA-950 laser diffraction particle size distribution analyser. Prior to measurement, subsamples were riffled down and treated with 0.1% hexametaphosphate, before dispersal in de-ionized water within the instrument using ultrasound and pumping. The resultant data were used to calculate the mean grain size of each sample, sorting, skewness, and kurtosis (Table S1).

Luminescence dating

Three approaches were taken to luminescence date the samples. Optically stimulated luminescence (OSL) on quartz extracts and infrared stimulated luminescence (IRSL) and post-infrared infrared stimulated luminescence (pIRSL) on feldspar extracts.

Samples MARY07115-1, 2 and 3 were prepared under subdued red lighting using standard preparation procedures (e.g. Bateman & Catt 1996; Spencer & Robinson 2008). Preliminary OSL quartz-based measurements were conducted at the St Andrews University luminescence laboratory using prepared 180–212 μm quartz mounted as a monolayer on 9.6-mm-diameter aliquots. Initial experiments on preheat and dose recovery were conducted to determine the appropriate preheat temperature and to determine whether a hot bleach was required

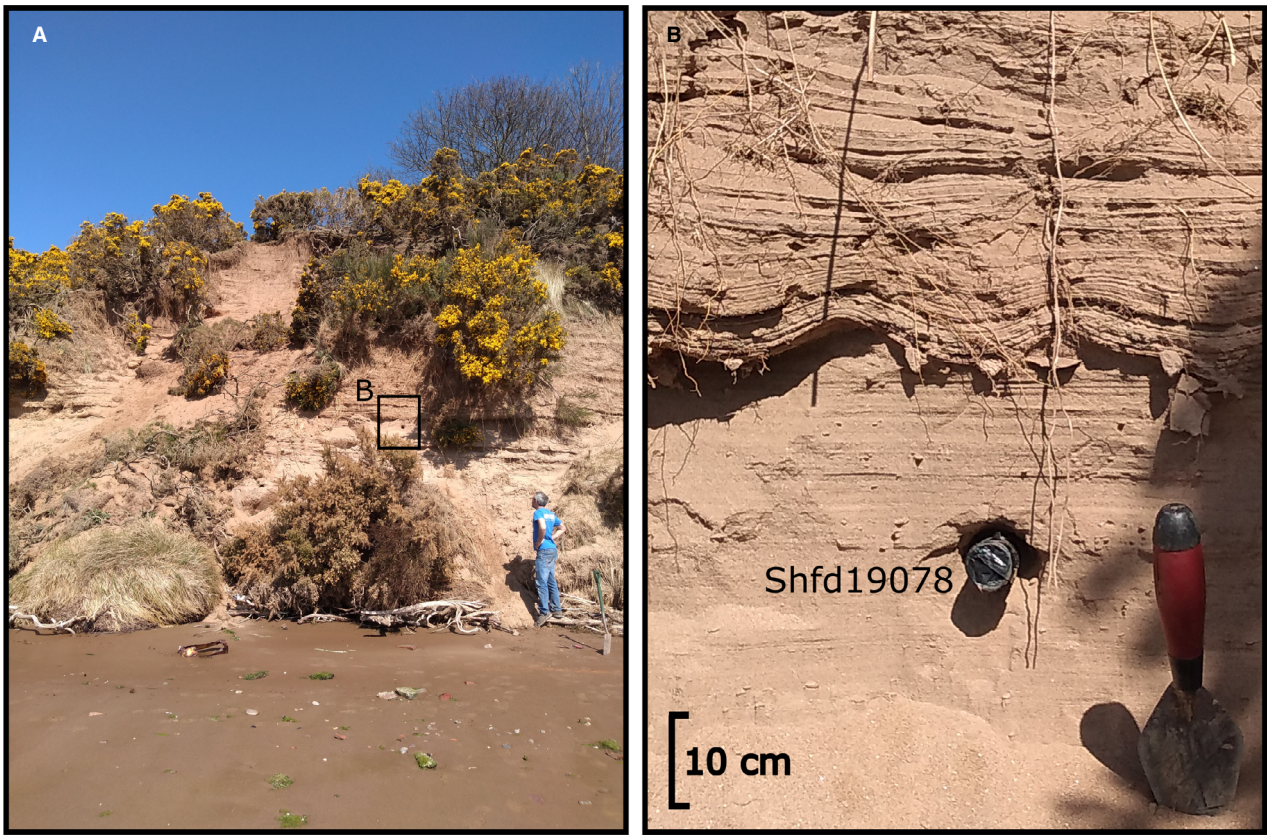

Fig. 4. Section through raised Pleistocene marine sediments at the Montrose Basin edge near the cemetery at Tayock.

for each sample. Measurements used the SAR protocol outlined by Murray & Wintle (2003), with six to seven regeneration points to characterize the OSL growth curve. Sample preheats were typically 240–260 °C for 10 s and cutheat 160 °C. For some samples, the SAR protocol was modified to include infrared stimulation before OSL to optically remove unwanted feldspar signals and an additional OSL bleach to remove luminescence due to thermal transfer. Further details on the protocol are in Spencer & Robinson (2008) and Morrocco *et al.* (2007). Between 50 and 75 replicates were measured for each sample (Table 2, Fig. S1). For these samples, estimation of dose rates were based on elemental concentrations as determined by ICP-MS and palaeomoistures based on present-day ones (Table 2).

All other OSL, IRSL and pIRSL measurements were undertaken at the Sheffield University luminescence laboratory. For both feldspar and quartz measurements, grains in 180–250 μm sand size range were mounted as a ~2-mm-diameter monolayer on 9.6-mm-diameter aliquots. For the OSL measurements, an experimentally derived preheat of 180 °C for 10 s was applied prior to SAR measurement and five regeneration points were used. Initial measurements using IR showed, despite HF etching, persistence of feldspar contamination believed to be from feldspar inclusions within the quartz (Fig. S2). To mitigate the effects of this, prior to each OSL measurement within SAR, a 60-s IR wash at 50 °C was applied. IRSL measurements were undertaken at 50 °C following a preheat of 250 °C for 60 s (Rhodes 2015). Between 48 and 96 replicate aliquots were measured for both OSL and IRSL to evaluate reproducibility and any potential partial bleaching issues (Fig. S3). The exception to this was the core sample, which was split into ~1-cm slices and each slice separately prepared and measured (Shfd17233–244).

pIRSL measurements followed the procedure initially outlined by Buylaert *et al.* (2012). It has been shown that IRSL and low temperature pIRSL measurements can be affected by anomalous fading leading to age underestimations (e.g. Buylaert *et al.* 2012; Rhodes 2015). This can be avoided by using higher temperatures. However, the IRSL signal stimulated at higher temperatures is less easily reset by exposure to sunlight in the natural environment so can be prone to age over-estimation due to only partial resetting. For the pIRSL measurements used here, following IRSL SAR measurement at 50 °C, the IRSL signal was re-measured with the sample held at an elevated temperature ranging from 180 to 290 °C. To establish an unbleachable residual dose, aliquots of feldspar were exposed to UK sunshine for 7 days and then measured using SAR. This resulted in a residual of

Table 2. OSL related data for sampled sites from Montrose Basin dunes.

Sample site/code	Material	Method	Depth from surface (m)	Alpha dose rate (μGy a^{-1})	Beta dose rate (μGy a^{-1})	Gamma dose rate (μGy a^{-1})	Cosmic dose rate (μGy a^{-1})	Total dose rate (μGy a^{-1})	*n*	D_e (Gy)	OD (%)	Age (a)[4]
Maryton												
MARY071105-1	Tsunami sand	SA-OSL	3.0	27±5	1404±112	832±53	141±7	2403±125[1]	51	18.10±1.72	22	7530±820
MARY071105-2	Tsunami sand	SA-OSL	3.5	28±6	1479±118	869±56	132±7	2508±131[1]	68	19.30±1.41	34	7700±690
MARY071105-3	Below tsunami	SA-OSL	4.08	25±5	1118±88	708±45	123±6	1975±99[1]	75	25.40±1.50	40	12 860±1000
Shfd17231	Tsunami sand	SA-$IRSL_{50}$	2.2	10±2	1775±100	881±58	156±8	2842±110	48	23.35±0.57	15	8660±420
Shfd17230	Tsunami sand	SA-OSL	2.2	10±2	1281±71	629±43	156±8	2076±102	43	16.99.0±0.46	23	8190±410
Shfd17230	Tsunami sand	SA-$IRSL_{50}$	2.2	10±2	1895±110	629±41	156±8	2690±1029	80	22.81±0.55	25	8480±380
Shfd17230	Tsunami sand	SA-$pIRSL_{180}$	2.2	10±2	1616±79	851±58	156±8	2651±99	55	31.3±0.14[2]	28	11 670±410
Shfd17230	Tsunami sand	SA-$pIRSL_{225}$	2.2	10±2	1616±79	851±58	156±8	2651±99	55	33.4±1.11[2]	29	12 460±600
Shfd17230	Tsunami sand	SA-$pIRSL_{290}$	2.2	10±2	1616±79	851±58	156±8	2651±99	7	75.84±5.39[2]	15	31 000±2300
Shfd17232–244	Tsunami sand	SA-OSL	2.2	10±2	1002±71	881±60	156±8	2067±93	5007	16.97±0.19	24	8210±380
Shfd17232–244	Tsunami sand	SA-$IRSL_{50}$	2.2	10±2	1616±79	851±58	156±8	2651±99	4970	21.46±0.5[3]	24	8000±350
Tayock												
Shfd19078	Marine sand	SA-$IRSL_{50}$	5.25	30±6	1377±100	854±39	106±5	3208±116	33	45.4±1.4	20	14 150±640
Shfd19078	Marine sand	SA-$pIRSL_{225}$	5.25	30±6	1377±100	854±39	106±5	3208±116	26	88.79±3.4[2]	26	27 680±1500

[1]Dose rate determined from ICP-MS elemental concentrations with palaeo-moisture as measured during sampling.
[2]An experimentally determined residual of 5.64 Gy (for 180 °C) and 7.21 Gy (for 225 and 290 °C) was subtracted from the measured D_e to obtain the value presented.
[3]D_e determined using the minimum age model as data skewed.
[4]Ages presented in years from the year 2020 rounded to the nearest decade and with 1 sigma uncertainties.

5.64 Gy for 180 °C pIRSL measurements and 7.21 Gy for pIRSL measurements at 225 and 290 °C.

Dose rates for the samples measured at Sheffield had their external gamma dose rates based on the field gamma spectrometry measurements. External beta dose rates were based on ICP-MS elemental measurements converted to dose rates using data from Guérin *et al.* (2011) and appropriately attenuated for grain size and density. A palaeomoisture value of 26% was determined based on present-day moisture levels with a 2% error to incorporate fluctuations through time (Table 2). An internal dose rate from the feldspars subjected to IRSL and pIRSL was based on an assumed internal potassium content of 12% (Rhodes 2015). A cosmogenic dose rate contribution was calculated as per Prescott & Hutton (1994).

Measured palaeodose (D_e) replicates generally showed low overdispersion (OD) with normal distributions. Given this, the samples are considered to have been sufficiently reset (bleached) at deposition and final D_e values for age calculation purposes were derived using the central age model of Galbraith & Green (1990). Ages are reported with one sigma confidence levels. The exception to this was the subsampled 'slices' from Shfd17232–244, and the combined IRSL D_e distribution, which was skewed. The combined age is, therefore, based on a D_e extracted using the minimum age model (Galbraith *et al.* 1999).

Numerical modelling

Hill *et al.* (2014) employed an area wide model to model the Storegga event up to but not inundating the coastlines of the North Sea and beyond. To provide more detail on the potential coastal impact of the tsunami a small regional model incorporating inundation was undertaken for the areas around the Firth of the Forth and Tay Estuaries including the Montrose Basin (Fig. 5). The landscape for the model used OS Terrain 5 DTM topography (5-m resolution) and Marine DEM 1 arc second bathymetry (resolution ~30 m) from OS (2018a, b). This was adjusted for glacial isostatic changes using the GIA model output of Bradley *et al.* (2011) and the sea level curves of Shennan *et al.* (2018) to produce a palaeobathymetry DEM. A 20-m contour was used as the coastal boundary, to allow for inundation, with a curved boundary from south to north of the domain that acted as a forced boundary. All mapping and transformation of spatial data were carried out in QGIS (QGIS 2020) and converted to formats suitable for meshing using qmesh (Avdis *et al.* 2018). Two-dimensional Delaunay triangulation was used to generate a mesh (Geuzaine & Remacle 2009) that had a resolution of 100 m up to 500 m from the coastal boundary. This was followed by a linear increase to 5-km resolution 50 km from the landward boundary, after which it stayed at this. The resolution from the forcing boundary was 1 km up to 3 km from the boundary, with a linear increase to 5-km resolution at 50 km from the boundary. An additional metric was employed as a function of depth via a sigmoidal function. Model resolution, therefore, varied from around 100 m in shallow regions near the landward boundary to 5 km in deeper water away from any boundary. DEM data were interpolated onto this mesh via HRDS (Hill 2019) via bilinear interpolation. For the inundation model Thetis, a 2D and 3D flow solver implemented using the Firedrake finite element solver (Angeloudis *et al.* 2018; Kärnä *et al.* 2018; Harcourt *et al.* 2019), was used.

Thetis solves the shallow water equations:

$$\frac{\partial \eta}{\partial t} + \nabla \cdot (H_d \mathbf{u}) = 0, \tag{1}$$

$$\frac{\partial \mathbf{u}}{\partial t} + \mathbf{u} \cdot \nabla \mathbf{u} - \nu \nabla^2 \mathbf{u} + f \mathbf{u}^{\perp} + g \nabla \eta = \frac{-\tau_b}{\rho H_d}, \tag{2}$$

where η is the free surface perturbation, t is time, H_d is the total water depth and $\mathbf{u}$ is the depth-averaged velocity vector with horizontal components, $\mathbf{u}$, v while ν is the kinematic viscosity of the fluid. Also, $f\mathbf{u}^{\perp}$ accounts for the Coriolis effect and comprises of $\mathbf{u}^{\perp}$, the velocity vector rotated counter-clockwise over 90° and $f = 2\Omega\sin(\zeta)$ with Ω the angular frequency of the Earth's rotation and ζ the latitude. Also, g is the gravitational acceleration (m s^{-2}), τ_b is the bed shear stress and ρ is the fluid density (kg m^{-3}). Manning's drag equation from Angeloudis *et al.* (2018) was also used:

$$\frac{\tau_b}{\rho} = g n^2 \frac{\|\mathbf{u}\|\mathbf{u}}{H_d^{\frac{1}{3}}}, \tag{3}$$

where n is the Manning coefficient of 0.03. The wetting and drying algorithm used in Thetis is from Kärnä *et al.* (2011). The model was run with the alpha parameter for wetting and drying set at 10, with a viscosity of 1 m^2 s^{-1} and a timestep of 3 s. Model data were outputted every 60 s, with a total runtime of 5 h simulated time. Boundary conditions on the eastern side were derived from Hill *et al.* (2014), which used a solid-block model of the Storegga tsunami. The model outputted bathymetry, maximum depth, maximum elevation, free surface elevation (wave height) and the velocity. The maximum depth and bathymetry were used to show the inundation of the wave.

Results

Sediment characterization

ICP-MS analyses of the Maryton samples (Table 3) showed distinct differences between the silts and the tsunami sands (Fig. 6A). Whilst this may in part reflect

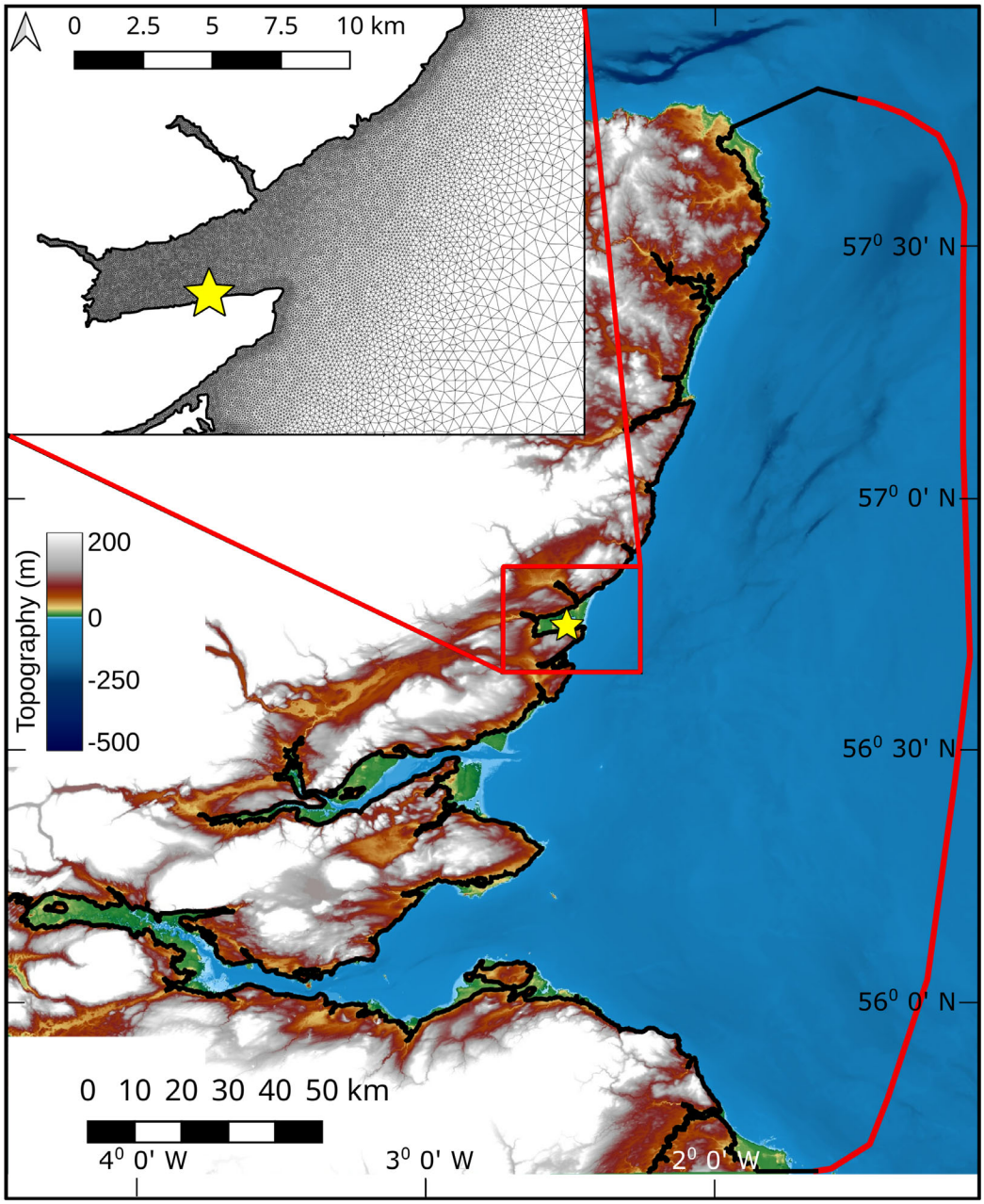

Fig. 5. Map of the modelled domain covering most of NE Scotland. The Maryton site is highlighted with a star. Red line on the right shows the marine boundary that is used to input the Storegga tsunami wave from Hill *et al.* (2014), the black lines are the other model boundaries, including the palaeo-20 m contour. Inset shows detail of the 2D mesh used in the area of interest.

the difference in particle size, it could indicate a change in provenance. As shown in Table 4, the average Ti/Zr and Ti/Nb ratios are essentially identical, indicating that the minerals containing Ti have been broken down and removed. The ratio elements usually associated with immobile minerals, such as zircons (Dunajko & Bateman 2010; Carr *et al.* 2019), suggest the tsunami sand is most similar to the Pleistocene raised marine sands (Zr/Hf) or beach sand (La/Yb). Particle size indicates the mean grain size of the tsunami sand (96 μm) is least close to the beach (301 μm) and dunes (281 μm) and closest to the raised marine terrace sediments (mean ranges from 122 to 272 μm). The Rb/Sr and Ba/Sr ratios show the tsunami sand to be similar to the other sands, indicating similar weathering levels (Brookfield *et al.* 2019). Separation is more apparent when the tri-plots are examined (Fig. 6B) as these clearly indicate that the tsunami sediment is closest to the raised marine beach and dune sand but distinctive from them. The enhanced Zr and Hf concentrations indicate an

older/more mature source for the tsunami sand than the source of the estuarine silts, which were being deposited immediately before and after the tsunami event. The Cr/Th ratio of 124 makes the tsunami sand distinctly different to any of the other deposits tested with values exceeding the upper continental crust (7.76; McLennan *et al.* 2006). Such a ratio indicates some igneous silicate (mafic) input (Ali *et al.* 2014).

As would be expected the estuarine silts and tsunami sands show very different particle size characteristics (Table S1, Fig. 7A). The estuarine silts above and below the tsunami sand both have similar average mean diameters (30 and 32 μm), identical sorting (1.19) and similar kurtosis (1.06 and 1.00) and skewness (0.16 and 0.12). This makes them both poorly sorted, medium silts that are slightly positively skewed (i.e. with a finer tail) and mesokurtic. They represent similar depositional environments before and after the tsunami with, based on the Hjulström's curve, depositional water velocities of <0.2 cm s^{-1} indicative of limited wave action. In contrast, the tsunami sands have a mean diameter of 96 μm, sorting of 1.38, kurtosis of 1.25 and skewness of −0.36. This characterizes the sediment of this unit as a fine, poorly sorted sand that is negatively skewed (i.e. with a coarser tail) and leptokurtic. It represents higher energy deposits with depositional water velocities up to 5× that of the silts (Hjulström's curve indicates deposition at <1 cm s^{-1} water velocity).

As Fig. 7B shows, both the mean size and sorting indicate three fining-up successions with the middle dominating. Initially grains are coarser and more poorly sorted and as deposition continues these get finer and better sorted until the next succession starts. The basal succession starts with a mean of 116 μm and sorting of 1.42 and finishes with a mean of 56 μm and sorting of 1.30. The second starts with a mean of 141 μm and sorting of 1.36, which declines to a mean of 78 μm and sorting of 1.28. The final succession is less well developed and starts with a mean of 101 μm and sorting of 1.72 and finishes with a mean of 56 μm and sorting of 1.38. Comparisons between the three successions show that the first covers 5.7 cm of the unit, the second 9 cm of the unit and the third 2.4 cm of the unit. The second succession starts with the coarsest. Transitions from fine to coarse are very abrupt indicating no coarsening-up successions. Overall, there is a slight general fining from bottom to top of the tsunami sand.

Luminescence dating

Preliminary luminescence ages show that the estuarine silts had an age of 12 860±1000 years (MARY071105-3; Table 2) and the overlying tsunami sand ages of 7530 ±820 and 7700±690 years (MARY071105-1 and MARY071105-2, respectively; Table 2). Whilst within error of each other the uncertainties of the latter are quite large. To improve on this, further measurements were made at the small aliquot level with a gamma dose rate based on *in situ* measurements and employing both OSL on quartz and IRSL on feldspars. Results from sample Shfd17230 produced a quartz OSL age of 8190±410 years (Table 2). No OSL age is reported for Shfd17231 as a persistent signal from feldspar inclusions resulted in an unreliable estimate of D_e. $IRSL_{50}$ measurements for the

Table 3. Selected elemental concentrations from a range of potential sedimentary sources within the Montrose Basin as measured by ICP-MS.

Sampled unit	Ba (ppm)	Cr (ppm)	Sc (ppm)	Sr (ppm)	Ti (%)	Co (ppm)	Hf (ppm)	La (ppm)	Nb (ppm)	Rb (ppm)	Yb (ppm)	Th (ppm)	Zr (ppm)
Estuarine silt above	642	147	10	174	0.52	14.1	7	35	16	108	2.6	9.6	263
Estuarine silt above	624	114	12	175	0.54	15.6	7	39	16	120	2.9	11.3	293
Estuarine silt above	710	130	14	180	0.54	14.2	6	41	8	113	2.8	10.7	237
Tsunami sand top	570	360	12	180	0.48	11.2	8	31	12	88	2.6	8.3	318
Tsunami sand	430	810	8	190	0.5	6.9	12	17	12	53	2.2	5.2	500
Tsunami sand	420	660	8	190	0.52	6.7	12	18	14	50	2.4	5.4	513
Tsunami sand	380	730	9	190	0.6	7.5	16	18	15	47	2.8	5.1	664
Tsunami sand	360	880	9	180	0.65	7.7	17	18	16	42	3	5.4	785
Tsunami sand	360	840	10	180	0.68	8.2	23	20	16	43	3.2	6.1	955
Tsunami sand	420	770	8	190	0.52	7.3	13	18	13	50	2.4	5.2	560
Tsunami sand bottom	490	580	10	180	0.48	10.7	9	27	7	70	2.6	7.1	372
Estuarine silt below	640	130	15	170	0.53	14.7	5	42	10	119	2.6	11.2	207
Estuarine silt below	642	147	14	180	0.59	22	9	31	15	108	2.4	12.3	351
Estuarine silt below	733	141	16	178	0.55	24.4	7	56	16	135	3.1	13.9	267
Estuarine silt below	701	141	10	202	0.5	13	8	35	15	104	2.7	10.2	319
Raised marine sand	386	319	6	154	0.28	9.6	3	17	7	59	1.6	5.2	133
Raised marine sand	383	308	7	162	0.36	9.4	7	22	9	59	2.0	6.9	291
Raised marine sand	412	341	8	174	0.41	12.5	7	22	11	61	1.9	6.4	333
Modern beach	326	506	<5	156	0.13	4.9	2	10	4	51	0.8	3.3	102
Modern beach	300	327	<5	152	0.14	4.4	2	9	4	46	0.8	2.9	78
Modern dune	307	559	<5	136	0.15	5.6	2	10	4	46	0.9	3.3	92
Modern dune	316	575	<5	153	0.19	5.4	3	12	5	45	1.3	4	112

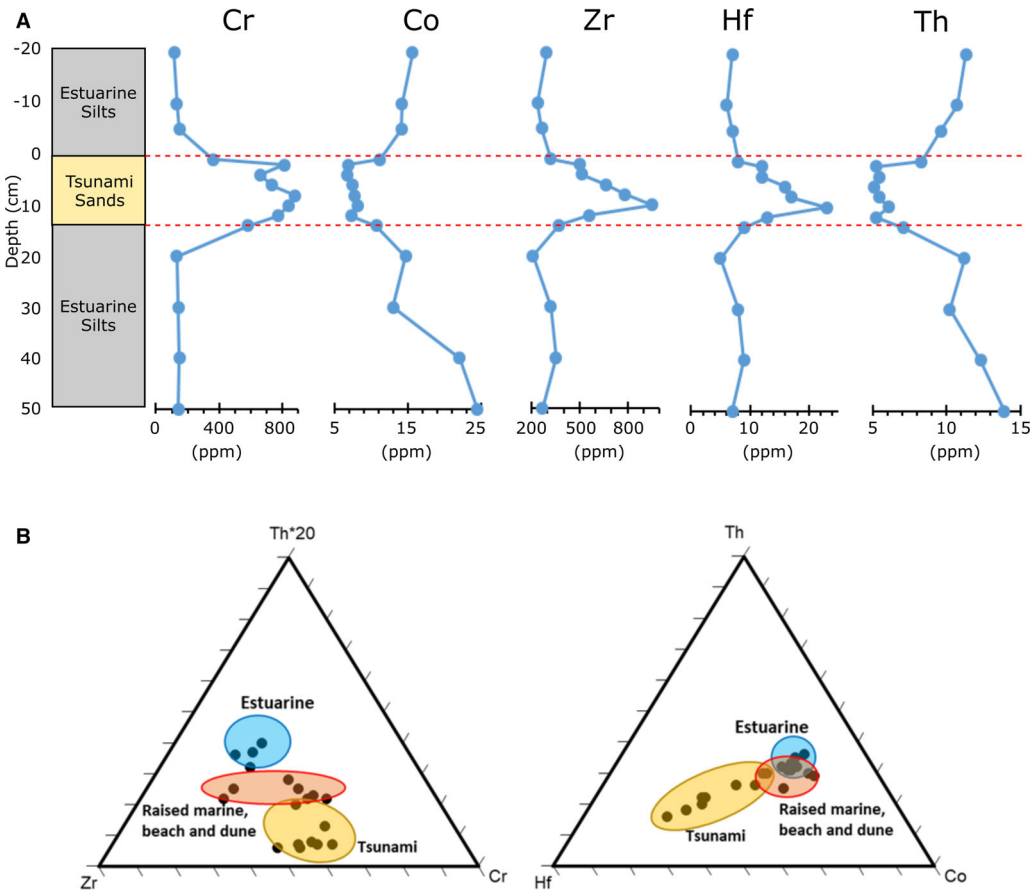

Fig. 6. Geochemical provenance analysis. A. Selected elements as measured by ICP-MS demonstrating a clear difference in geochemistry between the Montrose estuarine sediments and the tsunami sands. B. Tri-plots of key elements, which show tsunami sands are enriched in Hf and Zr and from a mature source most similar to the raised marine, beach and dune sediment.

2017 bulk samples produced ages of 8480±380 and 8660 ±420 years (Shfd17230 and Shfd17231, respectively). That the two different minerals and methods agree indicates good signal resetting prior to deposition as feldspars reset slower (Bateman 2019; Fig. 2).

In addition to issues of feldspar inclusions in the quartz OSL, ICP-MS indicated high variability of potassium (K), uranium (U) and thorium (Th) within the tsunami unit that could have impacted the beta dose rate. To mitigate against this and improve upon the above ages further, samples Shfd17232 to 17244 were based on the whole tsunami sand unit. Up to 48 replicates for both $IRSL_{50}$ and OSL measurements were undertaken for each of the 12 subsamples spanning the entire tsunami unit (Fig. 8). With such a large D_e population it was hoped that the influence of any occasional individual aliquot suffering from feldspar inclusions or partial resetting would be minimized. Beta dose-rate variability was mitigated for by averaging the results from six ICP-MS samples, which covered the whole tsunami unit (Table S2). The D_e results from the quartz and feldspar subsamples were combined to produce a single D_e for

Table 4. Average elemental ratios from tsunami sand and a range of potential sedimentary sources within the Montrose Basin as measured by ICP-MS.

	Zr/Hf	Ti/Zr	Cr/Co	Ti/Nb	Cr/Th	La/Yb	Rb/Sr
Estuarine silt above	39.6±1.8	0.002±0.000	9.0±1.3	0.04±0.02	12.5±2.1	13.8±0.5	0.6±0.0
Tsunami sand	42.2±1.8	0.001±0.000	90.2±28.5	0.05±0.01	124.4±38.7	38.7±8.4	0.3±0.1
Estuarine silt below	39.0±0.7	0.002±0.000	7.8±2.2	0.04±0.00	12.0±1.5	14.6±2.4	0.7±0.1
Pleistocene marine sand	42.4±1.3	0.002±0.001	12.1±2.3	0.04±0.01	18.5±5.5	12.1±4.2	0.4±0.1
Modern beach	44.9±6.1	0.002±0.000	28.0±1.5	0.03±0.00	42.1±2.7	8.2±3.1	0.3±0.0
Modern dune	41.6±4.3	0.002±0.000	23.6±0.4	0.04±0.00	35.9±3.4	12.6±0.3	0.3±0.0

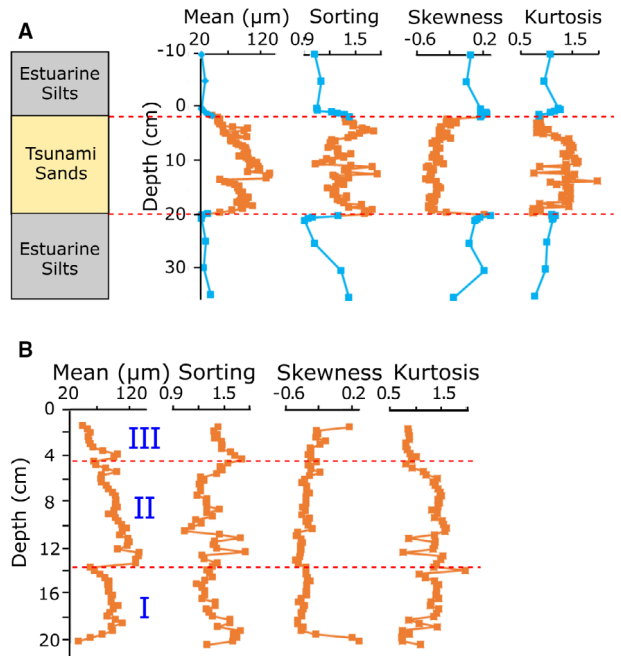

Fig. 7. Particle size analysis used to determine number of waves. A. Particle size analysis showing difference between tsunami sands and over- and underlying strata. B. Tsunami sand particle size data showing triplicate fining-up successions with associated cycles of sorting interpreted as the result of three tsunami waves.

both $IRSL_{50}$ and OSL to which the revised dose-rate was applied to calculate ages. This produced ages for samples Shfd17233 to 17244 of 8210±380 and 8000±350 years for OSL and $IRSL_{50}$, respectively. Given these ages are based on the analysis of the entire tsunami deposit, 500 and 497 D_e measurements from quartz and feldspar, respectively, and the beta dose rate evaluation is improved, combining these ages with the more limited data from samples Shfd17230 and Shfd17231 was not considered appropriate. Combining the quartz and feldspar ages from samples Shfd17233–244 (using OxCal v4.3; Bronk Ramsey 2009) led to a final age for the tsunami deposit at Maryton of 8100±250 years.

Luminescence was also used in a novel way to provide provenance information. Elemental analysis (as discussed above) indicated that the raised marine sand found on the northeast of the Montrose Basin may have been the source of the tsunami sands (Figs 2, 4). An $IRSL_{50}$ age of 14 140±640 years (Shfd19078) was determined for the near basal sample collected from the marine sands at Tayock showing that these sediments were emplaced prior to the tsunami and, therefore, could have been eroded during it. To establish if this was the source of the tsunami sediments, higher temperature pIRSL was undertaken on samples from both Maryton and Tayock. The principle behind this is that the higher temperature pIRSL signals would take longer to reset when exposed to sunlight. Whilst the OSL and IRSL data showed these two very light sensitive signals were reset through sunlight exposure, in a rapid tsunami event lasting only hours it is much less likely that higher temperature pIRSL signals would be. If no resetting occurred, ages calculated from $pIRSL_{180}$, $pIRSL_{225}$ and $pIRSL_{290}$ measurements from the Maryton samples could indicate the original age of the sediment from which the tsunami eroded. As shown in Table 2 sample Shfd17230 gave ages of 11 670±410, 12 460±600 years for $pIRSL_{180}$ and $pIRSL_{225}$, respectively, both within error of each other. This is similar to the age of the Tayock marine sediments (14 140±640 years) especially if it is considered that the tsunami would have eroded stratigraphically higher and younger sediments laid down to the east. Also of note is the coincidence of the ages (within errors) from the hardest to reset $pIRSL_{290}$ signal. These were 31 000±2300 years at Maryton and 27 680±1500 years at Tayock.

Numerical modelling

The regional inundation model produced two waves in total, one small initial wave and a second larger wave. The initial wave was the first wave to propagate out from the slide towards Iceland and Greenland. The larger second wave was due to refraction around the Shetland Isles. The maximum run-up for the tsunami was 3.89 m, which lies within the wave height range found by other studies (Bondevik *et al.* 2005b) but lower than most of the previously reported tsunami deposits (e.g. Long *et al.* 2016). Video of the full model simulation is available in the Supporting Information (Figs S4, S5).

With the new modelling, regionally the height of the second wave was greatest in the Montrose Basin at 3.64 m (Fig. 9A). The locations within the Montrose Basin also experienced the highest velocity (1.3 m s^{-1}) during the drawdown phase, with a second peak of 0.67 m s^{-1} on the incoming wave (Fig. 9B). As a result, the calculated BSS, when using the highest velocity on the incoming wave was around 1.1 N m^{-2} at its peak but only around 0.12 N m^{-2} sustained. A BSS of this magnitude would have been capable of transporting sediment between fine gravel and fine sand in size (Fig. 9B; Berenbrock & Tranmer 2008).

The modelled inundation that occurred at Montrose was mainly to the northwest of the basin (Fig. 10) where it penetrated up to 18 km inland. The only site inundated by the model where tsunami sediments have been reported is at Maryton. This location was reached by a wave of around 40 cm in height.

Discussion

Can tsunami sediments be accurately dated by luminescence?

The new direct luminescence age from the tsunami sediments at Maryton gave an age of 8100±250 years

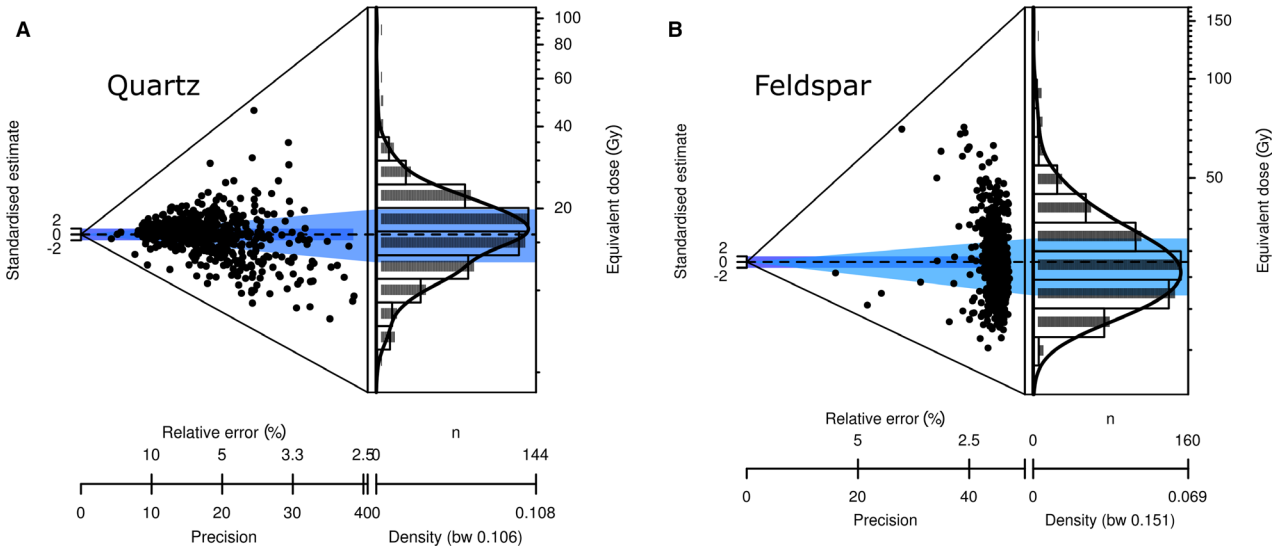

Fig. 8. Abanico plots of D_e distributions for Maryton tsunami samples showing low overdispersion interpreted as indicating good bleaching of the luminescence signal in the tsunami sediments prior to burial.

(Fig. 11). Recalibration (using IntCal13) of previously reported radiocarbon dates at Maryton (allowing a 77-year delay in recommencement of peat accumulation as per Smith *et al.* 2004) dates the tsunami to between 7997 ±250 and 8120±210 cal. a BP (Beta 92235, 92236; Smith *et al.* 2004). So, notwithstanding the comments of Dawson *et al.* (2011), the OSL and radiocarbon chronology at Maryton are within errors although the latter is a little younger suggesting the 77-year delay might be too small. The new luminescence age also compares well with the latest Storegga AMS dates from Norway of 8150 ±30 cal. a BP (Bondevik *et al.* 2012).

Given the coincidence of ages from feldspar and quartz with different bleaching characteristics, the low D_e scatter (overdispersion) for samples and the high number of replicates, the tsunami sediments found at Maryton appear to have been well bleached and so high precision luminescence ages could be obtained. Thus the biggest question of applying luminescence to tsunami sediments, i.e. that of bleaching, is overcome. That good bleaching occurred provides potential further insights into the tsunami event. Given the short transport pathway of the sediment moved in the event, the thinness of deposits associated with each wave (see section below) and rapid burial, sediment bleaching must have occurred during transport. The high levels of bleaching measured imply that sediment loading in the water during the tsunami was not high. Also, it has been suggested the tsunami occurred in October/November (Rydgren & Bondevik 2015) when daylight hours in Scotland are reduced to only ~9–11 h a day. Our results further suggest that the tsunami must have occurred during the day.

This study suggests that for successful dating of tsunami deposits using luminescence, a single horizontal sample should not be considered the optimum, as it has potential to enclose sediment from multiple waves and/or sample horizons potentially less well reset. Single grain D_e measurements might help isolate grains that were better bleached (and identify those that were poorly reset at deposition), but beta dose heterogeneity issues would still be unknown. An alternative, sampling tsunami deposits as monoliths or vertical cores – as illustrated in this study – ensures that the entirety of the deposit is analysed. D_e measurement of a large number of very small aliquots and multiple measurements of the beta dose rate through the deposit can help mitigate the effect of beta heterogeneity whilst retaining some ability to isolate any results from poorly reset grains. It is also recommended that IRSL on feldspar, and OSL on quartz are both carried out, as this facilitates comparisons of the different bleaching rates. As elsewhere in Scotland fine-medium grained sandy deposits have also been reported for Storegga tsunami deposits. A similar careful and high-resolution approach would be able to evaluate whether these have bleached sediments and could provide accurate OSL ages. It also provides confidence that application of luminescence dating to other less well chronologically constrained palaeo-tsunami deposits has the potential to provide accurate ages.

What was the direction and number of tsunami waves and what was the provenance of the tsunami sediment deposited at Maryton?

That the sediments at Tayock were deposited prior to the tsunami, and the Maryton and Tayock sediments share residual ages (i.e. $pIRSL_{180}$, $pIRSL_{225}$ and $pIRSL_{290}$), is taken as evidence that the raised Pleistocene marine sediments were the source of the sediment found at Maryton. The Maryton $pIRSL_{180}$ and $pIRSL_{225}$ ages of

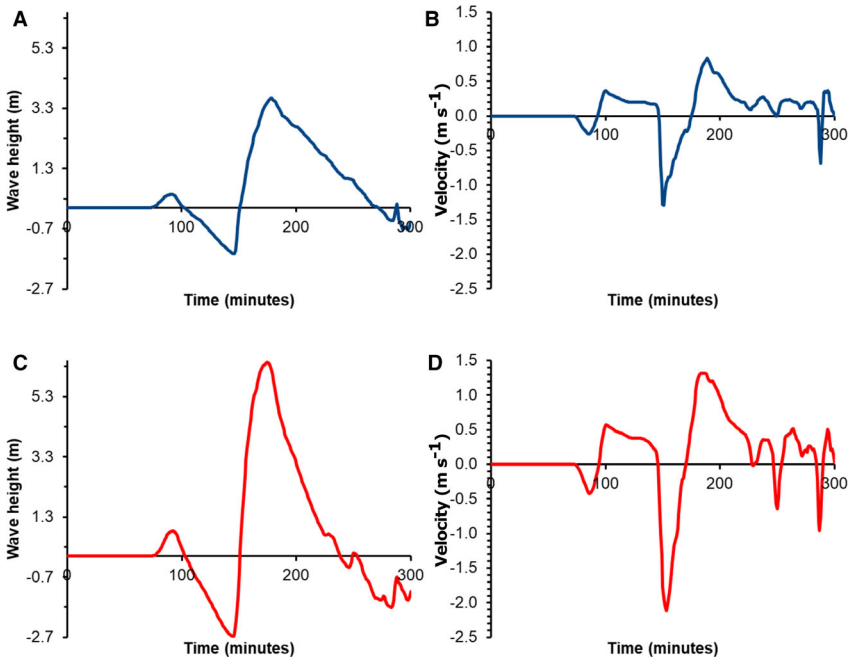

Fig. 9. Modelled Storegga wave outputs for Montrose Basin. A and B. Modelled with isostatically adjusted present-day topography. C and D. Modelled with Holocene marine sediments found across Montrose Basin entrance removed.

11 670±410, 12 460±600 years, respectively, are similar to the $IRSL_{50}$ age of 14 140±640 years from Tayock, especially when it is considered that the latter was a near basal sample and tsunami erosion would more likely have been on younger stratigraphically higher sediment closer to the sea (Fig. 11). At this time, sediment accumulation at Maryton was estuarine silt (MARY071105-3, Fig. 11). The synchronicity of the $pIRSL_{290}$ ages for Maryton and Tayock, which are based on the hardest to reset $pIRSL_{290}$ signals, provide additional support to this hypothesis. The geochemistry and particle size data also indicate this, but with an additional input of weathered mafic material. The source of the latter could be the Montrose Volcanic Formation, part of the Arbuthnott-Garvock Group and comprised of andesites and basalts, which underlies the Quaternary unconsolidated sediments on the coastal plain to the south and northeast of the basin (Phillips 2004).

To transport sediment from the Pleistocene raised marine sands, which would have formed the coastline at that time, and from the Montrose Volcanic Formation rocks to Maryton, the tsunami waves must have had to come from the east or northeast. One further line of evidence supports this. The Arbuthnott-Garvock Group has high chromium concentrations, which contrasts with the low chromium levels of the Strathmore Group sandstones, which underlie at depth the current Montrose Basin entrance to the east (Dochartaigh *et al.* 2006; BGS 2011). This would explain the contrast in Cr levels seen in the estuarine sediment above and below the tsunami deposit. The former would have been derived from tidal water coming from the east (low chromium) whereas the tsunami wave over-rode weathered Arbuthnott-Garvock group and marine sands to the northeast (high chromium). Smith *et al.* (2007) speculated that Montrose sediment was locally derived and this seems to be borne out by the data presented above.

The high-resolution particle size analysis of the tsunami sand at Maryton indicated three fining-up successions. These are interpreted as indicating that sediment deposition occurred as the waves moved onshore, with finer grain fractions settling out as wave(s) velocity dropped. If correct, three waves impacted on Maryton. Smith *et al.* (2007), based on contiguous 1-cm samples as opposed to the 2-mm samples of this study, identified only two fining-up successions for Maryton. Further inland they identified two fining-up and one coarsening-up succession at Fullerton and one fining-up succession at Old Montrose. Of the identified waves at Maryton it would appear that the second had the highest velocity as the deposit is coarsest and carried more sediment as this is the thickest of the fining-up successions. The sharp boundaries between the successions are taken to indicate water returning seaward before the next wave arrived. Smith *et al.* (2007) argued that the lack of change in sorting towards the surface of the sediment unit indicated deposition occurred well below the water

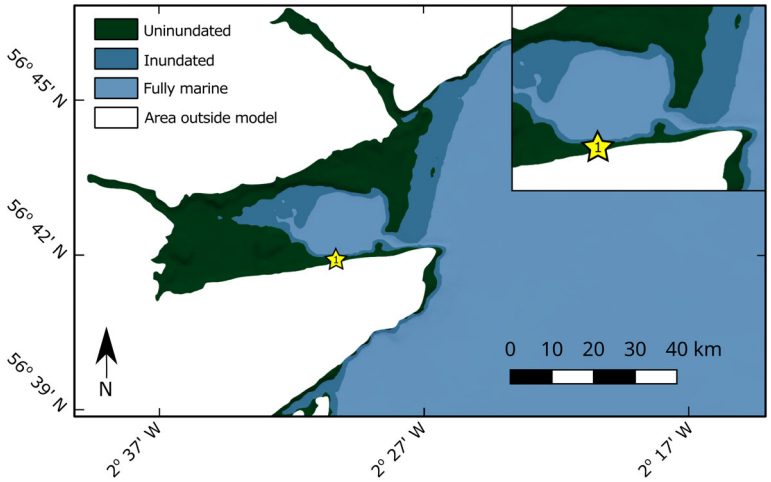

Fig. 10. Inundation of the model into the Montrose Basin using the bathymetry and maximum depth. Light blue shows the fully marine conditions, dark blue the inundated areas and dark green areas are the modelled land that never gets inundated. The study site at Maryton is marked by the star and also shown in inset.

surface (i.e. relatively deep water) and the new results from Maryton are consistent with this.

In summary, the tsunami interrupted low energy estuarine sedimentation. It came from the NE or E, over-ran pre-existing marine sands and weathered igneous bedrock which would have formed the beach and coastline at that time to the north of Montrose. The tsunami transported the marine sands and weathered bedrock across to Maryton and beyond. Three waves impacted on the coastline with the second being the largest in terms of energy and sediment load. Other estuaries in Scotland could be expected to have been impacted in the same way with local coastal sediments eroded and transported short distances.

Can modelling accurately replicate the tsunami impacts in the Montrose Basin?

The model successfully predicts a tsunami moving down the coastline from the northeast and impacting on the Montrose Basin. It also predicts a single large wave entering the Montrose Basin that takes considerable time to drain (~2 h). The wave direction within the basin is primarily westward on inflow (88° west) and eastwards on the outflow (89° east). There are subsequent smaller waves caused by reflections of the primary wave. This primary wave generates velocities capable of moving up to fine gravel for a short period, but predicts sustained transport of medium sand, which is consistent with the new sedimentological data presented above. However, of the six sites known to have preserved tsunami sediments, only one site (Maryton) is modelled to have been inundated. At the time of the tsunami, Maryton was just below sea level so it is not hard for the model to predict inundation (Fig. 11). Similar to the model of Hill *et al.* (2014), modelled wave height estimates appear, even with the extra coastal inundation modelling, to under-estimate wave run-up compared to the sedimentary record. For example, at Fullerton the run-up was estimated at 3.93 m (Smith *et al.* 2004) compared to the modelled wave height of 1.68 m. It should also be noted that the sedimentary evidence is probably an under-estimate of true tsunami run-up so modelled run-ups should, if anything, be higher than the sedimentary record. Smith *et al.* (2007) estimated a water run-up in the Montrose Basin of 11.2 m in places.

Two reasons can be put forward for the model's apparent under-estimation of run-up. Firstly, tsunami deposits found at Fullerton where the maximum observed run-up was found are situated in a gully (Fig. 2; Smith *et al.* 2007) where increased localized run-up of the tsunami could have taken place. This has been used to explain why run-ups of >30 m have been found on the Shetlands (Dawson *et al.* 2020). Such small-scale topographic modelling would be computationally difficult to incorporate accurately. Secondly, the under-estimation at Montrose could be due to the use of present-day topography as the starting point for the palaeobathymetry used in the model. The modelled restricted entrance to the Montrose Basin is nearly perpendicular to the direction of the wave and limited the amount of water inundating the basin as the wave would have had to refract around the coastline (Wei *et al.* 2013). This refraction when combined with the shallow water setting would have decreased the tsunami wave height and velocity (Ris *et al.* 1994) reducing the inundation distance predicted by the model. Evidence for an under-estimation of wave velocity is shown by the particle size of the tsunami sediments at Maryton, which have a mean of 100 μm and have 10% of grains >200 μm requiring a BSS of >0.145 N m^{-2} to transport (Berenbrock & Tranmer 2008). The modelled BSS for Maryton was below this

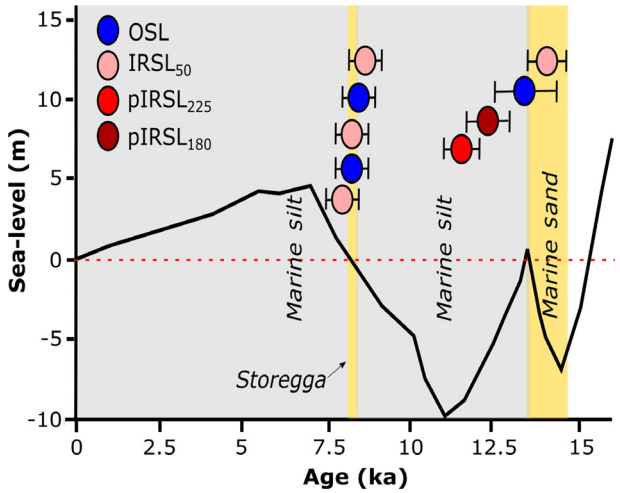

Fig. 11. Luminescence ages for sediment deposition at Montrose compared to modelled sea-level changes (as per Shennan *et al.* 2018) and basin sediments. Note ages plotted at arbitrary sea-level heights.

value for most of the time the incoming wave passed over the site implying only fine sand should have been deposited during inundation.

Evidence exists that the Montrose Basin may have been a more open embayment. Boreholes sunk during bridge construction in 2002 at the entrance to the Montrose Basin indicate bedrock (sandstone) outcrops below −24 m a.s.l. (BGS NO75NW21; Borehole A on Fig. 2). Boreholes in the Montrose town area between the basin and the sea indicate that this peninsular at least down to sea level is comprised of sands, gravels, silts and clays. For example, Borehole B on Fig. 2 (BGS NO75NW6853/8) logged 17 m of sand and rounded sands and gravels without hitting bedrock or any glacial sediments. The entrance to the Montrose Basin is, therefore, only blocked by unconsolidated sediment, which British Geological mapping indicates as Holocene marine. Given that relative sea level at Montrose was above that of present from 7 ka until recently, it is likely these Holocene marine sediments post-date the tsunami (Fig. 2). Mapped Holocene marine units give an indication of how far the palaeo-coastline has extended since then so this is relatively easily redefined. However, unlike the Lisbon tsunami record of 1755 where archaeological evidence can provide an exact elevation of the land surface at the time (e.g. Conde *et al.* 2015), this information is not easily derived for 8100 years ago. One solution would be to assume a present-day gradient with 0 m a.s.l. located at the Holocene–Pleistocene unit boundaries.

Accordingly, the palaeobathymetry was adjusted by lowering the area between the North Esk Estuary to the South Esk Estuary in Montrose mapped by the British

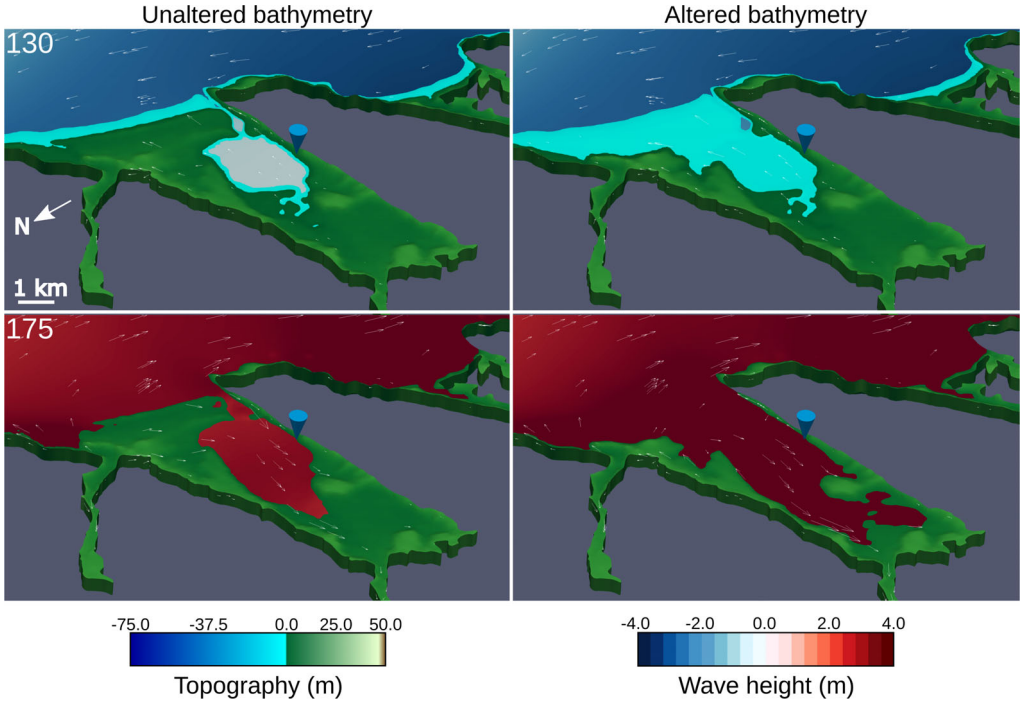

Fig. 12. Snapshots showing water level and topography comparing the simple reconstruction (left) vs. the removal of the beach-blown sand at the entrance of the Montrose Basin (right). The two snapshots shown correspond to roughly the minimum (top) and maximum (bottom) inundation and are approximately 9.8 (130 outputs) and 11.3 h (175 outputs) after slide initiation. The effect of a more open entrance to the Montrose Basin is clear. Video of the full model simulation is available in Figs S6, S7.

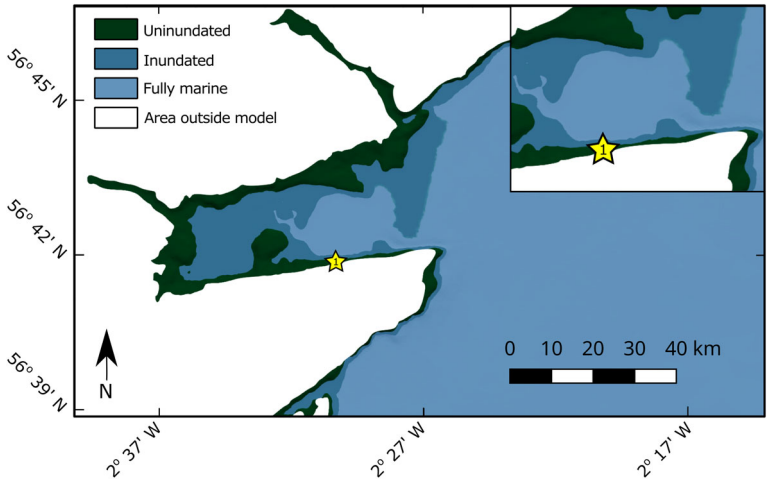

Fig. 13. Inundation of the model into the Montrose Basin using the bathymetry and maximum depth but revised with Holocene sediments found across the entrance to the Montrose Basin removed. The study site at Maryton is marked by the star and also shown in inset. In this revised model, all sites reported with tsunami sediments are inundated.

Geological survey as blown sand and beach/tidal flat deposits to 0 m a.s.l. Video of the full revised model simulation is available in Figs S6, S7 and model output is shown in Fig. 12. The new model produces a much more extensive inundation area (Fig. 13) with water penetrating inland >30 km. It also produces a wave that drains much more rapidly (Fig. 9D). The peak wave height increases inundating Maryton to a depth of over 3.2 m, compared to around 0.4 m without this modification (Fig. 9A, C). With a peak wave height of 6.45 m, the revised model also inundates five of the six sites reported to have tsunami sediments (Fullerton is not inundated but is thought to have had a larger run-up due to being in a gully). As such the revised model reconciles with the sedimentological evidence apart from number of waves. The model predicts two waves whilst the sedimentary evidence suggests a third less well-developed fining-up succession. A very minor third wave is modelled (Fig. 9 D) which, with further refinement of the palaeobathymetry, might become more significant. Alternatively, the less well-developed sedimentary fining-up succession may reflect a very localized refractive wave within the Montrose embayment.

Although somewhat crude, the altered bathymetry indicates the importance of reconstructing the palaeotopography/bathymetry when modelling palaeo-tsunamis. In doing so, it holds the key to better being able to model the inundation extents and impacts of palaeo-tsunami waves along coastlines. Given the on-going postglacial isostatic uplift of Scotland, emergence of new coastal sediments is widespread as sea level has fallen although these new coastal configurations are not necessarily well constrained temporarily. Further work is required to establish how and when the North Sea coastline has evolved (including man-made structures) to better constrain future models.

Conclusions

- Use of feldspars and quartz, high numbers of replicates and detailed dose rate evaluation allowed the luminescence data combined with sedimentological data to show good bleaching prior to burial and to be successfully applied to the tsunami sediments. Such an approach provides confidence that application of luminescence dating to other less well chronologically constrained palaeo-tsunami deposits has the potential to provide accurate ages.
- Tsunami deposits at Maryton date to 8100±250 years. This is concordant with the bracketing radiocarbon chronology there and the date of the Storegga tsunami from Norway.
- In Maryton the tsunami interrupted quiet low energy estuarine sedimentation, came from the NE or E and over-ran and eroded pre-existing marine sands and weathered igneous bedrock on the coastal plain.
- Three waves impacted in the Montrose Basin with the second being the largest in terms of energy and sediment load.
- Multiple elevated temperature IRSL measurements can be used to help understand sediment transport histories and sedimentary sources.
- Incorporation of an inundation model into the tsunami model of Hill *et al.* (2014) is able to better replicate direction, number of waves and sediment size.
- Modelling shows that even when run at a local regional level topographic effects cannot be adequately replicated leading to persistent underestimation of wave run-up. To mitigate the effects of this palaeotopography and palaeo-near-shore bathymetry require careful consideration. With this, future model evolution will be better able to

inform on the hazard risk and potential impacts for future high-magnitude submarine generated tsunami events.

Acknowledgements. – Permission to sample at Montrose was given by Vanessa Kirkbride from Scottish Natural Heritage and the Scottish Wildlife Trust. Professor Sue Dawson is thanked for discussions on earlier versions of this research. Stein Bondevik and an anonymous reviewer are thanked for their time and constructive comments. No conflicts of interest are declared.

Author contributions. – MDB, TCK, RBIB and RR participated in the fieldwork and sampling. MDB, TCK, RAA and RR undertook the luminescence dating and sediment characterization. JH and JM undertook the inundation modelling. MDB, TCK, RBIB and JH took part in the scientific discussions and helped with the writing and editing of the manuscript.

Data availability statement. – The data that support the findings of this study are available from the corresponding author upon reasonable request.

References

Ali, S., Stattegger, K., Garbe-Schönberg, D., Frank, M., Kraft, S. & Kuhnt, W. 2014: The provenance of Cretaceous to Quaternary sediments in the Tarfaya basin, SW Morocco: evidence from trace element geochemistry and radiogenic Nd–Sr isotopes. *Journal of African Earth Sciences 90*, 64–76.

Angeloudis, A., Kramer, S. C., Avdis, A. & Piggott, M. D. 2018: Optimising tidal range power plant operation. *Applied Energy 212*, 680–690.

Avdis, A., Candy, A. S., Hill, J., Kramer, S. C. & Piggott, M. D. 2018: Efficient unstructured mesh generation for marine renewable energy applications. *Renewable Energy 116*, 842–856.

Bateman, M. D. 2019: Applications in glacial and periglacial environments. *In* Bateman, M. D. (ed.): *The Handbook of Luminescence Dating*, 191–221, Whittles Publishing, Dunbeath.

Bateman, M. D. & Catt, J. A. 1996: An absolute chronology for the raised beach and associated deposits at Sewerby, East Yorkshire, England. *Journal of Quaternary Science 11*, 389–395.

Berenbrock, C. & Tranmer, A. W. 2008: Simulation of Flow, Sediment Transport, and Sediment Mobility of the Lower Coeur d'Alene River, Idaho. Table 7. *Scientific Investigations Report* 2008-5093. US Geological Survey, Reston, Virginia.

BGS 2011: 1:250,000 Offshore Sea Bed Sediment Types. UK, British Geological Survey, EDINA Geology Digimap Service, Using http://edina.ac.uk/digimap.

Bondevik, S., Lovholt, F., Harbitz, C., Mangerud, J., Dawson, A. G. & Svendsen, J. I. 2005a: The Storegga Slide tsunami – comparing field observations with numerical simulations. *Marine and Petroleum Geology 22*, 195–208.

Bondevik, S., Mangerud, J., Dawson, S., Dawson, A. G. & Lohne, O. 2005b: Evidence for three North Sea tsunami at the Shetland Isles between 8000 and 1500 years ago. *Quaternary Science Reviews 24*, 1757–1775.

Bondevik, S., Stormo, S. K. & Skjerdal, G. 2012: Green mosses date the Storegga tsunami to the chilliest decades of the 8.2 ka cold event. *Quaternary Science Reviews 45*, 1–6.

Bondevik, S., Svendsen, J. I., Johnsen, G., Mangerud, J. & Kaland, P. E. 1997: The Storegga tsunami along the Norwegian coast, its age and runup. *Boreas 26*, 29–53.

Bradley, S. L., Milne, A. G., Shennan, I. & Edwards, R. 2011: An improved glacial isostatic adjustment model for the British Isles. *Journal of Quaternary Science 26*, 541–552.

Brill, D., Klasen, N., Brückner, H., Kruawun, J., Scheffers, A., Kelletat, D. & Scheffers, S. 2012: OSL dating of tsunami deposits from Phra THONG Island, Thailand. *Quaternary Geochronology 10*, 224–229.

Bronk Ramsey, C. 2009: Bayesian analysis of radiocarbon dates. *Radiocarbon 51*, 337–360.

Brookfield, M. E., Stebbins, S. G., Williams, W. S., Wolbach, W. S., Hannigan, R. & Bhat, G. M. 2019: Palaeoenvironments and elemental geochemistry across the marine Permo-Triassic boundary section, Guryul Ravine (Kashmir, India) and a comparison with other North Indian passive margin sections. *The Depositional Record 6*, 75–116.

Buylaert, J. P., Jain, M., Murray, A. S., Thomsen, K. J., Thiel, C. & Sohbati, R. 2012: A robust feldspar luminescence dating method for Middle and Late Pleistocene sediments. *Boreas 41*, 435–451.

Carr, A. S., Bateman, M. D., Cawthra, H. C. & Sealy, J. 2019: First evidence for onshore marine isotope stage 3 aeolianite formation on the southern Cape coastline of South Africa. *Marine Geology 407*, 1–15.

Conde, D. A. S., Telhado, M. J., Baptista, M. A. V. & Ferreira, R. M. 2015: Severity and exposure associated with tsunami actions in urban waterfronts: the case of Lisbon, Portugal. *Natural Hazards 79*, 2125–2144.

Dawson, A. G., Bondevik, S. & Teller, J. T. 2011: Relative timing of the Storegga submarine slide, methane release, and climate change during the 8.2 ka cold event. *The Holocene 21*, 1167–1171.

Dawson, A. G., Dawson, S., Bondevik, S., Costa, P. J. M., Hill, J. & Stewart, I. 2020: Reconciling Storegga tsunami sedimentation patterns with modelled wave heights: a discussion from the Shetland Isles field laboratory. *Sedimentology 67*, 1344–1353.

Dawson, A. G., Long, D. & Smith, D. E. 1988: The Storegga Slide: evidence from eastern Scotland for a possible tsunami. *Marine Geology 82*, 271–276.

Dunajko, A. C. & Bateman, M. D. 2010: Sediment provenance of the Wilderness barrier dunes, southern Cape coast, South Africa. *Terra Nova 22*, 417–423.

Firth, C. R., Smith, D. E., Hansom, J. D. & Pearson, S. G. 1996: Holocene spit development on a regressing shoreline, Dornoch Firth, Scotland. *Marine Geology 124*, 203–214.

Fruergaard, M. S., Piasecki, P., Johannessen, N., Noe- Nygaard, T., Andersen, M., Pejrup, M. & Nielsen, L. 2015: Tsunami propagation over a wide, shallow continental shelf caused by the Storegga Slide, southeastern North Sea, Denmark. *Geology 43*, 1047–1050.

Gaffney, V., Fitch, S., Bates, M., Ware, R. L., Kinnaird, T., Gearey, B., Hill, T., Telford, R., Batt, C., Stern, B., Whittaker, J., Davies, S., Sharada, M. B., Everewtt, R., Cribdon, R., Kistler, L., Harris, S., Kearney, K., Walker, J., Muru, M., Hamilton, D., Law, M., Finlay, A., Bates, R. & Allaby, R. G. 2020: Multi-proxy characterisation of the Storegga Tsunami and its impact on the Early Holocene landscapes of the southern North Sea. *Geosciences 10*, 270, https://doi.org/10.3390/geosciences10070270.

Galbraith, R. F. & Green, P. F. 1990: Estimating the component ages in a finite mixture. *Nuclear Tracks and Radiation Measurements 17*, 197–206.

Galbraith, R. F., Roberts, R. G., Laslett, G. M., Yoshida, H. & Olley, J. M. 1999: Optical dating of single and multiple grains of quartz from Jinmium rock shelter, northern Australia, part I: experimental design and statistical models. *Archaeometry 41*, 339–364.

Gale, S. J. & Hoare, P. G. 1991: *Quaternary Sediments*. 323 pp. Belhaven Press, London.

Geuzaine, C. & Remacle, J.-F. 2009: Gmsh: a 3-D finite element mesh generator with built-in pre- and post-processing facilities. *International Journal for Numerical Methods in Engineering 79*, 1309–1331.

Gordon, J. E. 1993: Maryton (GCR ID: 184). *In* Gordon, J. E. & Sutherland, D. G. (eds.): *Quaternary of Scotland*, 2731–2735. *Geological Conservation Review Series 6*. Springer, Dordrecht.

Guérin, G., Mercier, N. & Adamiec, G. 2011: Dose-rate conversion factors: update. *Ancient TL 29*, 5–8.

Haflidason, H., Lien, R., Sejrup, H. P., Forsberg, C. F. & Bryn, P. 2005: The dating and morphometry of the Storegga Slide. *Marine and Petroleum Geology 22*, 123–136.

Harbitz, C. B., Løvholt, F. & Bungum, H. 2014: Submarine landslide tsunami: how extreme and how likely? *Natural Hazards 72*, 1341–1374.

Harbitz, C. B., Løvholt, F., Pedersen, G. & Masson, D. G. 2006: Mechanisms of tsunami generation by submarine landslides: a short review. *Norwegian Journal of Geology 86*, 255–264.

Harcourt, F., Angeloudis, A. & Piggott, M. D. 2019: Utilising the flexible generation potential of tidal range power plants to optimise economic value. *Applied Energy 237*, 873–884.

Hill, J. 2019: HRDS: a Python package for hierarchical raster datasets. *Journal of Open Source Software 4*, 1112, https://doi.org/10.21105/joss.01112.

Hill, J., Collins, G. S., Avdis, A., Kramer, S. C. & Piggot, M. D. 2014: How does multiscale modelling and inclusion of realistic palaeobathymetry affect numerical simulation of the Storegga Slide tsunami? *Ocean Modelling 83*, 11–25.

Ishizawa, T., Goto, K., Yokoyama, Y. & Goff, J. 2020: Dating tsunami deposits: present knowledge and challenges. *Earth-Science Reviews 200*, 102971, https://doi.org/10.1111/sed.12724.

Jaffe, B. E., Goto, K., Sugawara, D., Richmond, B. M., Fujino, S. & Nishimura, Y. 2012: Flow speed estimated by inverse modelling of sandy tsunami deposits: results from the 11 March 2011 tsunami on the coastal plain near the Sendai Airport, Honshu, Japan. *Sedimentary Geology 282*, 90–109.

Kärnä, T., de Brye, B., Gourgue, O., Lambrechts, J., Comblen, R., Legat, V. & Deleersnijder, E. 2011: A fully implicit wetting-drying method for DG-FEM shallow water models, with an application to the Scheldt Estuary. *Computational Methods in Applied Mechanical Engineering 200*, 509–524.

Kärnä, T., Kramer, S. C., Mitchell, L., Ham, D. A., Piggott, M. D. & Baptista, A. M. 2018: Thetis coastal ocean model: discontinuous Galerkin discretization for the three-dimensional hydrostatic equations. *Geoscientific Model Development 11*, 4359–4382.

Long, A. J., Barlow, N. L. M., Dawson, S., Hill, J., Innes, J. B., Kelham, C., Milne, F. D. & Dawson, A. 2016: Lateglacial and Holocene relative sea-level changes and first evidence for the Storegga tsunami in Sutherland, Scotland. *Journal of Quaternary Science 31*, 239–255.

Long, D., Smith, D. E. & Dawson, A. G. 1989: A Holocene tsunami deposit in eastern Scotland. *Journal of Quaternary Science 4*, 61–66.

McLennan, S. M., Taylor, S. R. & Hemming, S. R. 2006: Composition, differentiation and evolution of continental crust: constrains from sedimentary rocks and heat flow. *In* Brown, M. & Rushmer, T. (eds.): *Evolution and Differentiation of the Continental Crust*, 92–134. Cambridge University Press, Cambridge.

Morrocco, S. M., Ballantyne, C. K., Spencer, J. Q. G. & Robinson, R. A. L. 2007: Age and significance of aeolian sediment reworking on high plateaux in the Scottish Highlands. *The Holocene 17*, 349–360.

Muhs, D. R. & Budahn, J. R. 2006: Geochemical evidence for the origin of late Quaternary loess in central Alaska. *Canadian Journal of Earth Science 43*, 323–337.

Murray, A. S. & Wintle, A. G. 2003: The single aliquot regenerative dose protocol: potential for improvements in reliability. *Radiation Measurements 37*, 377–381.

Nath, B. N., Kunzendorf, H. & Pluger, W. L. 2000: Influence of provenance, weathering, and sedimentary processes on the elemental ratios of the fine-grained fraction of the bedload sediments from the Vembanad Lake and the adjoining continental shelf, southwest coast of India. *Journal of Sedimentary Research 70*, 1081–1094.

Ó Dochartaigh, B. É., Smedley, P. L., Macdonald, A. M. & Darling, W. G. 2006: Baseline Scotland: the Lower Devonian aquifer of Strathmore. *British Geological Survey Commissioned Report CR/06/250N,* 60 pp.

OS 2018a: Land and Height data, Terrain 5 DTM. Ordnance Survey, GB. Using: EDINA Ordnance Survey Service. http://edina.ac.uk/digimap.

OS 2018b: Bathymetry data, Marine DEM 1. Ordnance Survey, GB. Using: EDINA Ordnance Survey Service. http://edina.ac.uk/digimap.

Phillips, E. 2004: Petrology of the sedimentary and igneous rocks from the Strathmore district (Sheet 57), Scotland. *British Geological Survey Internal Report IR/04/125*, 1–26.

Prescott, J. R. & Hutton, J. T. 1994: Cosmic ray contributions to dose rates for luminescence and ESR dating: large depths and long-term time variations. *Radiation Measurements 2/3*, 497–500.

QGIS 2020: *QGIS Geographic Information System. Open Source Geospatial Foundation Project*. https://qgis.org/en/site/

Rasmussen, H., Bondevik, S. & Corner, G. D. 2018: Holocene relative sea level history and Storegga tsunami run-up in Lyngen, northern Norway. *Journal of Quaternary Science 33*, 393–408.

Rhodes, E. J. 2015: Dating sediments using potassium feldspar single-grain IRSL: initial methodological considerations. *Quaternary International 362*, 14–22.

Ris, R., Holthuijsen, L. & Booij, N. 1994: A spectral model for waves in the near shore zone. *Coastal Engineering Proceedings 1*, 68–78.

Rydgren, K. & Bondevik, S. 2015: Moss growth patterns and timing of human exposure to a Mesolithic tsunami in the North Atlantic. *Geology 43*, 111–114.

Shennan, I., Bradley, S. L. & Edwards, R. 2018: Relative sea-level changes and crustal movements in Britain and Ireland since the Last Glacial Maximum. *Quaternary Science Reviews 188*, 143–159.

Shtienberg, G., Yasur-Landau, A., Norris, R. D., Lazar, M., Rittenour, T. M., Tamberino, A., Gadol, O., Cantu, K., Arkin-Shalev, E., Ward, S. N. & Levy, T. E. 2020: A Neolithic mega-tsunami event in the eastern Mediterranean: prehistoric settlement vulnerability along the Carmel coast, Israel. *PLoS ONE 15*, e0243619, https://doi.org/10.1371/journal.pone.0247953.

Smith, D. E. & Cullingford, R. A. 1985: Flandrian relative sea-level changes in the Montrose Basin Area. *Scottish Geographical Magazine 101*, 91–104.

Smith, D. E., Foster, I. D. L., Long, D. & Shi, S. 2007: Reconstructing the pattern and depth flow onshore in a palaeotsunami from associated deposits. *Sedimentary Geology 200*, 362–371.

Smith, D. E., Morrison, J., Jones, R. L. & Cullingford, R. A. 1980: Dating the main postglacial shoreline in the Montrose area, Scotland. *In* Cullingford, R. A., Davidson, D. A. & Lewin, J. (eds.): *Timescales in Geomorphology*, 225–245. Wiley, Chichester.

Smith, D. E., Shi, S., Cullingford, R. A., Dawson, A. G., Dawson, S., Firth, C. R., Foster, I. D. L., Fretwell, P. T., Haggart, B. A., Holloway, L. K. & Long, D. 2004: The Holocene Storegga Slide tsunami in the United Kingdom. *Quaternary Science Reviews 23*, 2291–2321.

Spencer, J. Q. G. & Robinson, R. A. J. 2008: Dating intramontane alluvial deposits from NW Argentina using luminescence techniques: problems and potential. *Geomorphology 93*, 144–155.

Sugawara, D., Goto, K. & Jaffe, B. E. 2014: Numerical models of tsunami sediment transport – current understanding and future directions. *Marine Geology 352*, 295–320.

Svendsen, J. I. & Mangerud, J. 1990: Sea-level changes and pollen stratigraphy on the outer coast of Sunnmøre, western Norway. *Norsk Geologisk Tidsskrift 70*, 111–134.

Taylor, S. R. & McLennan, S. M. 1985: *The Continental Crust: Its Composition and Evolution*. 302 pp. Blackwell Scientific, Oxford.

Vital, H. & Stattegger, K. 2000: Major and trace elements of stream sediments from the lowermost Amazon River. *Chemical Geology 168*, 151–168.

Wagner, B., Bennike, O., Cremer, H. & Klug, M. 2010: Late Quaternary history of the Kap Mackenzie area, northeast Greenland. *Boreas 39*, 492–504.

Wei, Y., Chamberlin, C., Titov, V. V., Tang, L. & Bernard, E. N. 2013: Modeling of the 2011 Japan tsunami: lessons for near-field forecast. *Pure and Applied Geophysics 170*, 1309–1331.

Weninger, B., Schulting, R., Bradtmoller, M., Clare, L., Collard, M., Edinborough, K., Hilpert, J., Joris, O., Niekus, M., Rohling, E. J. & Wagner, B. 2008: The catastrophic final flooding of Doggerland by the Storegga Slide tsunami. *Documenta Praehistorica 15*, 1–24.

Wolfe, S. A., Muhs, D. R., David, P. P. & McGeehin, J. P. 2000: Chronology and geochemistry of Late Holocene eolian deposits in the Brandon Sand Hills: Manitoba, Canada. *Quaternary International 67*, 61–74.

Supporting Information

Additional Supporting Information may be found in the online version of this article at http://www.boreas.dk.

Fig. S1. Abanico plots of D_e distributions for Maryton Tsunami samples measured in St Andrews using quartz single aliquot SAR OSL.

Fig. S2. Relationship of IR wash signal and OSL signal from the test dose measurements within the SAR protocol for quartz from sample Shfd17231. This relationship is taken to indicate that for this sample the IR wash prior to OSL measurement within the SAR protocol is not sufficiently removing all IR signal from feldspar inclusions. As a consequence, the D_e for this sample was a significant under-estimation to true burial D_e.

Fig. S3. Abanico plots of D_e distributions for Maryton Tsunami samples measured in Sheffield using quartz single aliquot OSL and feldspar single aliquot IRSL.

Fig. S4. Full regional simulation using the refined Hill *et al*. (2014) model incorporating a local inundation model.

Fig. S5. Full regional simulation using the refined Hill *et al*. (2014) model incorporating both a local inundation model and modified palaeotopography.

Fig. S6. 3D full simulation of Montrose Basin using the refined Hill *et al*. (2014) model incorporating a local inundation model.

Fig. S7. 3D full simulation of the Montrose Basin using the refined Hill *et al*. (2014) model incorporating both a local inundation model and modified palaeotopography.

Table S1. Particle size measurement results through the tsunami sand unit at Maryton.

Table S2. ICP analysis of key radioactive elements used to calculate the dose rate for luminescence showing variability through the Storegga tsunami sand found at Maryton.